Geomorphology 449 (2024) 109059

Contents lists available at ScienceDirect

Geomorphology

journal homepage: www.journals.elsevier.com/geomorphology

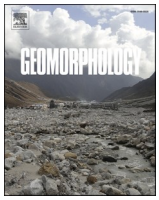

Landslides and growing folds: A lesson from the Kura fold-and-thrust belt (Azerbaijan, Georgia)

Tomáš Pánek [a,*], Michal Břežný [a], Hans-Balder Havenith [b], Alessandro Tibaldi [c]

[a] University of Ostrava, Department of Physical Geography and Geoecology, Chittussiho 10, Slezská Ostrava, Czech Republic
[b] Georisk and Environment, Department of Geology, University of Liège, Liège 4000, Belgium
[c] Department of Earth and Environmental Sciences, University of Milan-Bicocca, Milan, Italy

ARTICLE INFO

Keywords:
Landslides
Growing folds
Landslide inventory
Greater Caucasus
Kura fold-and-thrust belt

ABSTRACT

Active fold-and-thrust belts create new landslide-prone slopes during tectonic deformation propagation. However, studies on landslide distribution in newly formed fold-and-thrust belts are limited. In this study, we present a new inventory of landslides in the Kura fold-and-thrust belt, a tectonically active, but relatively low-altitude southern margin of the Greater Caucasus. The area has been tectonically framed in the last ~2–3 Ma and is represented by folds and thrusts deforming Miocene to Quaternary sediments. Through satellite imagery analysis, we mapped nearly 1600 landslides, with a quarter currently active. While landslides cover <1 % of the area, they tend to cluster at higher elevations and in regions with relatively high local relief. Landslides predominantly occur in tectonically uplifted areas, affecting the highest and steepest parts of growing anticlines and the steep slopes of incising valleys intersecting active thrust faults. Based on observed landslide distribution in folds at different stages of development, we propose a conceptual model for the temporal evolution of landslide patterns in weak sediment-based fold-and-thrust belts: 1) In the initial stages, slow-moving slope deformations affect incipient thrust fronts. With the flanks of the growing anticline lacking sufficient steepness, landslides tend to concentrate in deep valleys intersecting the uplifting hanging walls. 2) With ongoing thrust uplift, growing and steepening anticlines become more prone to planar sliding when dip slopes exceed friction angle, and valley development creates additional dip slopes, resulting in widespread landslides. 3) In the final stage, erosional decay reduces topographic relief, leading to badland formation with gully erosion and decreased landslide occurrence.

1. Introduction

Landslides are influenced by active tectonics in various ways (Bull, 2007). Tectonic activity has the potential to create favorable preconditions for landslides, such as weakened zones in bedrock (Korup, 2004) and steep slopes (Larsen and Montgomery, 2012). Moreover, active tectonics can directly trigger landslides through earthquakes (Tibaldi et al., 1995; Fan et al., 2019). Fold-and-thrust belts accommodate contraction at the front of collision mountains by formation of thrust faults and folds that propagate towards the adjacent basins (Hammerstein et al., 2020). As the folds grow in amplitude and propagate laterally, they can cause surface uplift (Keller et al., 1999). The uplift, coupled with the incision of the river network, generates new slopes that can be prone to mass movements. The interplay between tectonic deformation, surface uplift, newly generated topographic stresses and alterations in slope geometry consequently enhances the susceptibility of fold-and-thrust belts to landslides.

Many studies have been devoted to the evolution of the river valleys and drainage networks in evolving fold-and-thrust belts (e.g., Jackson et al., 1996; Hu et al., 2022), but investigations into slope stability on actively growing folds are relatively scarce. Exceptions are the few studies concerning landslides at the local scale of individual folds. For example, Hilley and Arrowsmith (2008) investigated landslide density in the Dragon's Back pressure ridge in California. They observed an increase in landslide density in the zone of greatest uplift, where the slopes of the fold were steep enough to cause slope instability. Similarly, Delchiaro et al. (2023) examined slope failure on the back limb of an anticline in the Zagros fold-and-thrust belt in Iran. They found that slope failure occurred when the limb angle reached a threshold due to fold growth. However, there is a lack of landslide inventories at the scale of

* Corresponding author.
E-mail address: tomas.panek@osu.cz (T. Pánek).

https://doi.org/10.1016/j.geomorph.2024.109059
Received 5 September 2023; Received in revised form 24 November 2023; Accepted 4 January 2024
Available online 10 January 2024

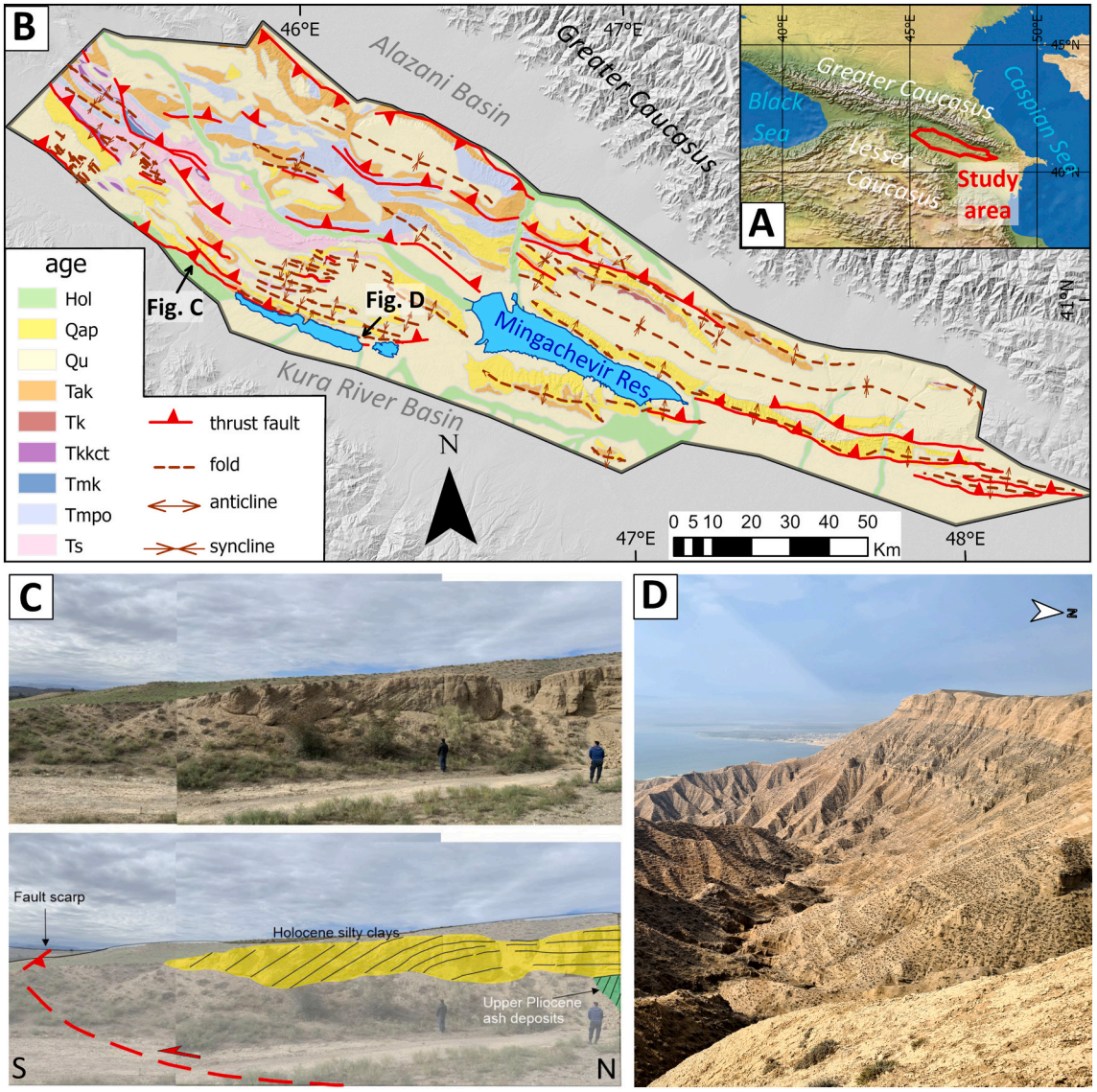

Fig. 1. Study area. A. Location of the Kura fold-and-thrust belt in the Caucasus orogen. B. Geology of the Kura fold-and-thrust belt (adapted from Nalivkin, 1976 and Forte et al., 2010, 2013). See Fig. 7 for abbreviations of age of lithostratigraphic units. C. Scarp of the Kura thrust with an outcrop of folded Late Quaternary alluvial deposits above the Kura River floodplain. D. Outcrop within the Apsheron lithostratigraphic unit composed of weakly indurated conglomerates and sands of Early Pleistocene age.

entire fold-and-thrust belts in the early stages of development, where deformation of Quaternary sediments occurs.

The Kura fold-and-thrust belt on the southeastern margin of the Greater Caucasus represents one of the youngest (<3 Ma; Forte et al., 2013; Sukhishvili et al., 2021) tectonic domains in the world and a major structural system that has recently accommodated convergence between Arabia and Eurasia (Forte et al., 2010). Despite the increasing number of studies focusing on neotectonics (Mosar et al., 2010; Forte et al., 2010, 2013, 2014; Alania et al., 2017; Sukhishvili et al., 2021; Pierce et al., in review) and lithostratigraphic evolution of the area (Forte et al., 2015), there is lack of papers dealing with geomorphic processes in the Kura fold-and-thrust belt (Sukhishvili et al., 2021). In addition, no attempts have been made to spatially assess landslides in this area, even though actively growing folds in the belt spatially overlap with Azerbaijan's critical infrastructure, such as the country's largest Mingachevir and Shamkir hydroelectrical water reservoirs. In any case, active tectonics and earthquakes significantly influence the distribution of landslides in the Greater Caucasus, as demonstrated by the 1991 Racha earthquake (Ms 7.0) in Georgia, which triggered landslides across an area exceeding 2500 km^2 and resulted in dozens of fatalities (Jibson et al., 1994).

This study represents the first attempt to investigate the spatial distribution of landslides across the majority of the Quaternary fold-and-thrust belt zone. The main objectives of this study are 1) to decipher the spatial distribution of landslides with the derivation of their main controls and 2) to relate the occurrence of landslides to active tectonic structures and the evolution of the Kura fold-and-thrust belt. We hypothesize that the spatial distribution of landslides in the area reflects different degrees of geomorphic development of folds and propagation of active structures into the foreland.

2. Regional settings

The study focuses on the eastern (~45°E–48°E) part of the Kura fold-and-thrust belt in Azerbaijan and Georgia (Fig. 1a). The elevation of the area reaches about 1000 m a.s.l. in the western part and decreases towards the east, where the ridges have an altitude of approximately 200 m a.s.l. Most of the area consists of hilly land, with valleys reaching a maximum depth of approximately 100 m. The area is bordered to the

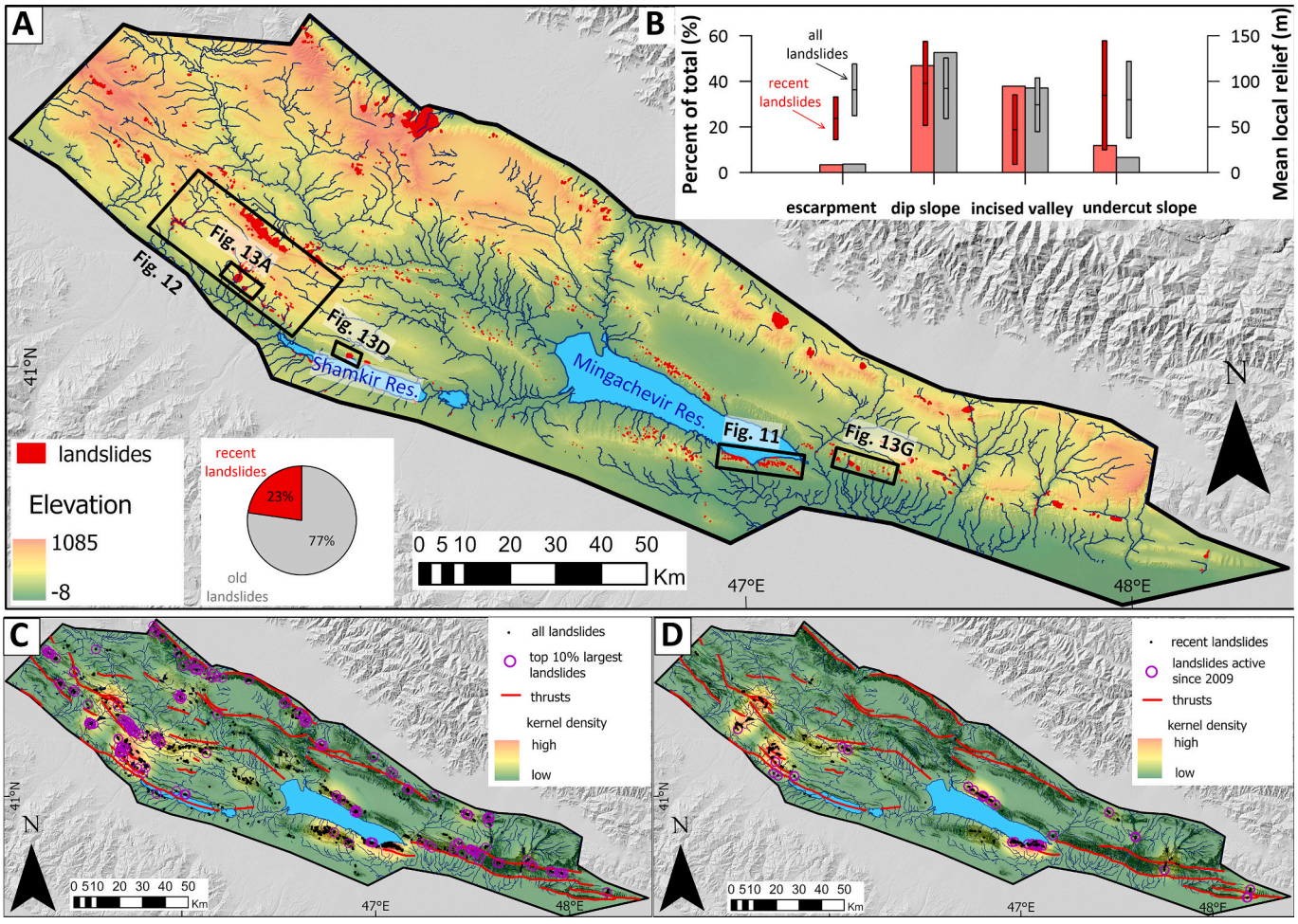

Fig. 2. Distribution of landslides in the Kura fold-and-thrust belt. A. Mapped landslides in the study area, with a pie chart indicating the proportion of recent and old landslides. B. Topographic settings and mean local relief (box plots with ±1σ) of inventoried landslides, displayed separately for the entire dataset and the subset of active landslides. C. Kernel density estimation of all recorded landslides within a 10-km radius window. D. Kernel density estimation of recent landslides within a 10-km radius window.

south by the Kura River valley and to the north by the Alazani River basin. The climate is moderately humid to semi-arid with annual rainfall exceeding 700 mm in the northern part and <300 mm along the Kura River valley in the south (Fick and Hijmans, 2017).

The Kura belt is a south-vergent, thin-skinned fold-and-thrust belt forming the southeast margin of the Greater Caucasus orogen (Shirinov and Bajenov, 1962; Borsuk and Sholpo, 1983; Forte et al., 2010). With a shortening rate between 6.7 and 13.6 mm/yr, the Kura fold-and-thrust belt is the main deformation zone between the Greater and Lesser Caucasus, accommodating ~30 %–40 % of the total convergence between Arabia and Eurasia since ~2–3 Ma (Forte et al., 2010, 2013). The belt displays a reduction in both width and elevation when progressing towards the east (Fig. 1b), indicating larger uplift and deformation in the western segment of the belt (Forte et al., 2013). The western part of the belt exhibits greater structural complexity, with over ten distinct folds, whereas the eastern part is composed of three folds plunging to the east (Forte et al., 2010).

The folds are accompanied by NW- to WNW-striking thrusts that dip to the north (Mosar et al., 2010; Forte et al., 2010, 2013). Notable examples of these faults include the Mingachevir thrust and the Kura thrust (Nalivkin, 1976; Forte et al., 2010) with the latter forming the youngest, southern margin of the belt above the Kura River valley (Fig. 1b). While only a few paleoseismic studies have been conducted in the area to determine the precise timing of the most recent tectonic events (Pierce et al., in review), the observed displacements of late Quaternary sediments along the Kura thrust indicate significant Holocene/recent tectonic deformation throughout the Kura fold-and-thrust belt (Fig. 1c). However, despite the occurrence of young tectonic deformation, no strong earthquakes (M > 6) have been recorded in the study area during the instrumental measurement period (Telesca et al., 2018; Fig. 1b). The last devastating earthquake with M ~ 7 hit the area in AD 1139 and destroyed the town of Ganja, the second largest town in Azerbaijan (Ismail-Zadeh et al., 2020). This earthquake likely had a limited impact on the southern part of the Kura fold-and-thrust belt, with more pronounced effects observed in the Lesser Caucasus. Here, it triggered two giant rock avalanches (with a total volume of at least 500 × 10^6 m^3) from the Kapaz Mountain (Nikonov and Nikonova, 1986; Havenith, 2022). Other strong earthquakes of comparable magnitude occurred in AD 1668 and 1902, with epicenters located near the town of Shamakhi, situated approximately 30 km east of the study area (Ismail-Zadeh et al., 2020).

The studied section of the Kura fold-and-thrust belt comprises Neogene and Quaternary sediments of the Kura River basin, forming a westward embayment of the Caspian basin system (Fig. 1b; Nalivkin, 1976; Forte et al., 2015). The western/higher part of the area is more exhumed, and the surface is primarily composed of Miocene sediments from the Sarmatian, Maeotian, and Pontian stages. The eastern half of the area is characterized by Pliocene and Pleistocene sediments from the Akchagyl and Apsheron Stages, which can reach several hundred meters to over a kilometer in thickness. (Forte et al., 2015). The individual

Table 1
Main characteristics of landslide inventory.

Landslide subset/number of landslides	Mean landslide area (m^2)	Median landslide area (m^2)	5 % quantile of landslide area (m^2)	95 % quantile of landslide area (m^2)	Mean elevation (m; ±1σ)	Mean local relief (m; ±1σ)	Mean slope (°; ±1σ)	Landslide types***	Geological units****
All landslides (n = 1575)	6.71×10^4	6.45×10^3	4.90×10^2	1.88×10^5	391 ± 173	85 ± 35	12.7 ± 4.4	PS (39 %), US (24 %), SS (20 %), RS (10 %), F (6 %), DG (<1 %)	Qap (33 %), Qu (24 %), Ts (18 %), Tak (14 %), Tmpo (7 %), Tkkct (1 %), Hol (1 %), Tmk (<1 %)
Recent landslides (n = 358)*	1.01×10^5	7.69×10^3	5.91×10^2	1.27×10^5	350 ± 149	95 ± 37	14.3 ± 4.8	PS (44 %), SS (21 %), US (14 %), RS (14 %), F (7 %)	Qap (43 %), Qu (23 %), Ts (18 %), Tak (8 %), Tmpo (3 %), Tkkct (2 %), Hol (2 %)
Post 2009 landslides (n = 47)**	1.39×10^4	5.82×10^3	4.08×10^2	4.91×10^4	247 ± 83	111 ± 33	16.6 ± 4.4	PS (66 %), F (13 %), US (11 %), SS (6 %), RS (4 %)	Qu (51 %), Qap (38 %), Tak (6 %), Hol (4 %)

* All landslides that show signs of current activity.
** Subset of recent landslides that have been dated using satellite imagery to the period after 2009.
*** PS – planar (slab) slides, US – undifferentiated slides, SS – shallow (debris) slides, RS – rotational slides, F – flows, DG – deep-seated gravitational slope deformations.
**** For abbreviations of geological units see Fig. 7.

geological units display intricate lithological sequences comprising conglomerates, sands, sandstones, muds, marls, and intermittent intercalations of carbonates and evaporites (Nalivkin, 1976; Forte et al., 2015). Towards the upper portions of the sequences, the formations tend to become coarser (Forte et al., 2013, 2015), resulting in topographic elevations predominantly composed of conglomerates or sandstones (Fig. 1d). The sediments within the Kura fold-and-thrust belt are primarily characterized as weak and poorly lithified. The majority of Pliocene and Quaternary sediments, including those from the Akchagyl and Apsheron stages, consist of unconsolidated sands, conglomerates, and muds (Fig. 1d).

Despite the potential susceptibility of the Kura fold-and-thrust belt to mass movements, there is currently no published inventory of landslides at the regional scale. More attention was paid only to landslides around the shoreline of Mingachevir reservoir (Yetirmishli et al., 2018). Several planar slides on the limbs of the anticline, which are susceptible to reactivations triggered by fluctuations in water levels, have been documented, particularly along the southern bank of the Mingachevir reservoir in close proximity to the dam site (Kotyuzhan and Molokov, 1990; Bairamov et al., 1992; Islamova et al., 2019).

3. Materials and methods

3.1. Landslide mapping

We conducted landslide mapping over an area of >13,000 km^2 in the eastern portion of the Kura fold-and-thrust belt, which is composed of Neogene and Quaternary sediments (Fig. 2a). As the majority of primary sources for high-resolution satellite images and digital elevation models (e.g., TanDEM-X) are restricted from public use due to ongoing war operations in the wider region, we primarily relied on freely available Google Earth™ imagery for landslide detection. Since over 95 % of the studied area lacks forest cover, the optical images available through Google Earth™ serve as a reliable source of information for mapping slope failures.

Landslides were mapped using common criteria for identification, such as the presence of arcuate scarps, tension cracks, closed depressions, bulges and lobate toes (Cruden and Varnes, 1996). During the mapping process, we distinguished between old landslides and recent ones displaying signs of active deformations. The recent landslides, estimated to be a few decades old at most, were identified by fresh scarps, cracks, lack of grass cover, and infrastructure damage. As a subset of the recent landslides, our focus was on identifying the newest ones that originated or were reactivated since 2009, aligning with the high-resolution satellite imagery timeframe in Google Earth™. When comparing images from before and after 2009, these landslides emerged as entirely new features or expanded from previously smaller failures. The landslides were categorized into three main groups: slides, flows, and slope deformations, as defined by Hungr et al. (2014). Slides encompass planar slides, rotational slides, shallow (debris) slides and unclassified slides. To verify the main types of landslides, field inspections were conducted in the western part of the study area in years 2022 and 2023. Additionally, we differentiated landslides based on their topographic locations, including dip slopes of anticlines, escarpments (located at the front of thrusts), deeply incised valleys, and undercut banks.

3.2. Landslide characteristics

The major topographic, geological, and climatic characteristics of landslides were obtained from available sources and analyzed spatially using standard tools in ArcGIS. The topographic characteristics were derived from the NASADEM Digital Elevation Model (DEM) with a resolution of 30 m, available at https://lpdaac.usgs.gov/products/nasadem_hgtv001/. Various topographic metrics were calculated, including elevation, local relief, slope, standard deviation of slope, difference between mean and minimum elevation (H_{mean}-H_{min}), hypsometric integral, and drainage density. These metrics were computed using focal statistics within a 250-m radius window. The choice of this window size was based on the relatively shorter slopes and lower topographic relief in the study area compared to mountainous regions, where larger search windows (typically 1–5 km) are commonly used (Montgomery and Brandon, 2002). To characterize the gradient of valleys adjacent to the mapped landslides, we also calculated the normalized channel steepness index (k_{sn}) (Kirby and Whipple (2012). We employed TopoToolbox (Schwanghart and Scherler, 2014) to preprocess the DEM using the carving method (Schwanghart and Scherler, 2017), generated a river network with a drainage area of at least 1 km^2, and calculated k_{sn} with the concavity index set to $\theta = 0.45$.

For geological characterization, we obtained information regarding the distribution of geological units from the 1:500,000 Geological Map of the Caucasus (Nalivkin, 1976). Information on active faults was retrieved from personal observations (Tibaldi et al., in review.) and various references, including Nalivkin (1976), Forte et al. (2010, 2013), and Alania et al. (2017). Information on the spatial distribution of annual rainfall and average rainfall of the wettest month for the period 1970–2000 was obtained from the WorldClim dataset (Fick and Hijmans, 2017).

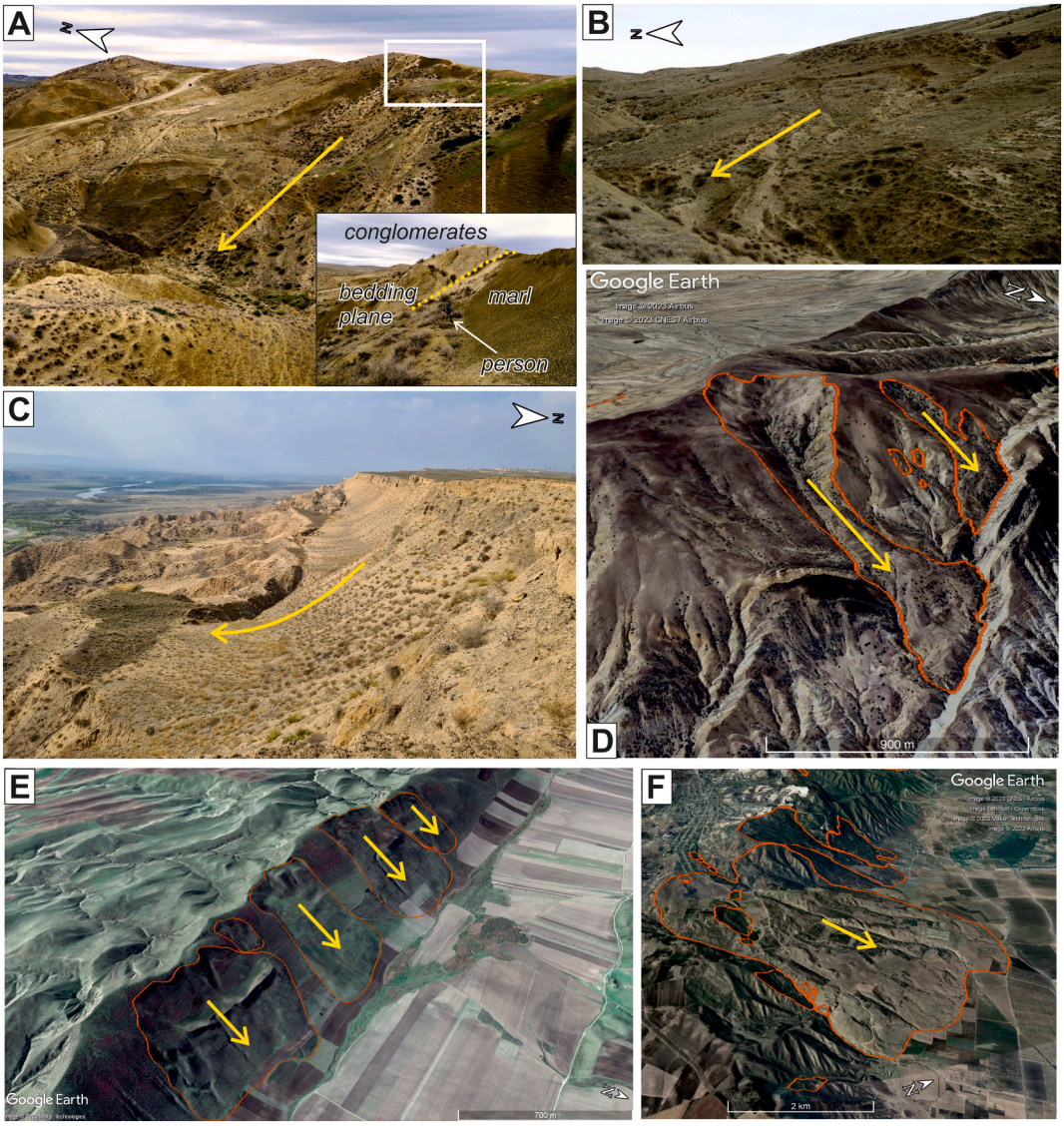

Fig. 3. Examples of landslides in the Kura fold-and-trust belt. A. Planar slide with a surface of rupture developed at the contact between conglomerates and marls of the Pliocene Akchagyl Formation (45.7349° E, 41.1669° N). B. Shallow planar debris slide affecting the dip slope of an anticline (45.8556° E, 41.1162° N). C. Rotational slide above the scarp of the Kura River, developed within the sands and conglomerates of the Early Pleistocene Apsheron Formation (45.9778° E, 41.0179° N). D. Earth flows developed within Miocene (Sarmatian) sediments (45.8801° E, 41.2206° N). E. Planar slides with morphology modified by agricultural activities (47.9651° E, 40.6603° N). F. The largest landslide in the study area (~24 km^2) developed on the escarpment of the inverted Didi Shiraki syncline above the Alazani Basin (46.1747° E, 41.4739° N).

3.3. Statistical analysis

We applied frequency-area statistics (Malamud et al., 2004) to characterize the mapped landslides, enabling a comparison of landslide size distribution across different inventories. The frequency density was calculated by dividing the number of landslides in each bin by the width of the bin, and the results were plotted against the lower boundary area of that bin. To test the validity of power-law fit, determine the cutoff position, and the exponent β of the negative power-law tail we utilized the poweRlaw package (Gillespie, 2015) in the R programming language (R Core Team, 2019). This package uses approach of maximum-likelihood fitting and goodness-of-fit test based on Kolmogorov-Smirnoff statistic proposed by Clauset et al. (2009). The frequency-area statistics allowed us to compare the distribution of the size between recent and old landslides, as well as assess the differences in landslide sizes based on their topographic positions. To infer the main controls on landslides and understand the structure in the relationships between variables, the distribution of landslides was investigated using a Principal Component Analysis (PCA). For this purpose, the study area was divided into a 10-km square grid, which was clipped by the area boundary and water reservoirs (Supplementary Fig. 1). We also excluded flat basin bottoms with a local relief <10 m, as these areas do not exhibit landslides. As a result, we obtained 135 polygons where we calculated the percentage of landslide coverage (dependent variable) along with a total of 16 standardized independent topographic, climatic, and geological variables. All topographic data, along with annual rainfall, average rainfall of the wettest month, and fault density, were used as average values, while lithology was expressed as % cover of a given geological unit (Fig. 1b) within the clipped 10-km squares.

4. Results

4.1. Landslide inventory

In total, we mapped 1575 landslides, which cover <1 % of the Kura fold-and-thrust belt study area (Fig. 2a). Slides are by far the most

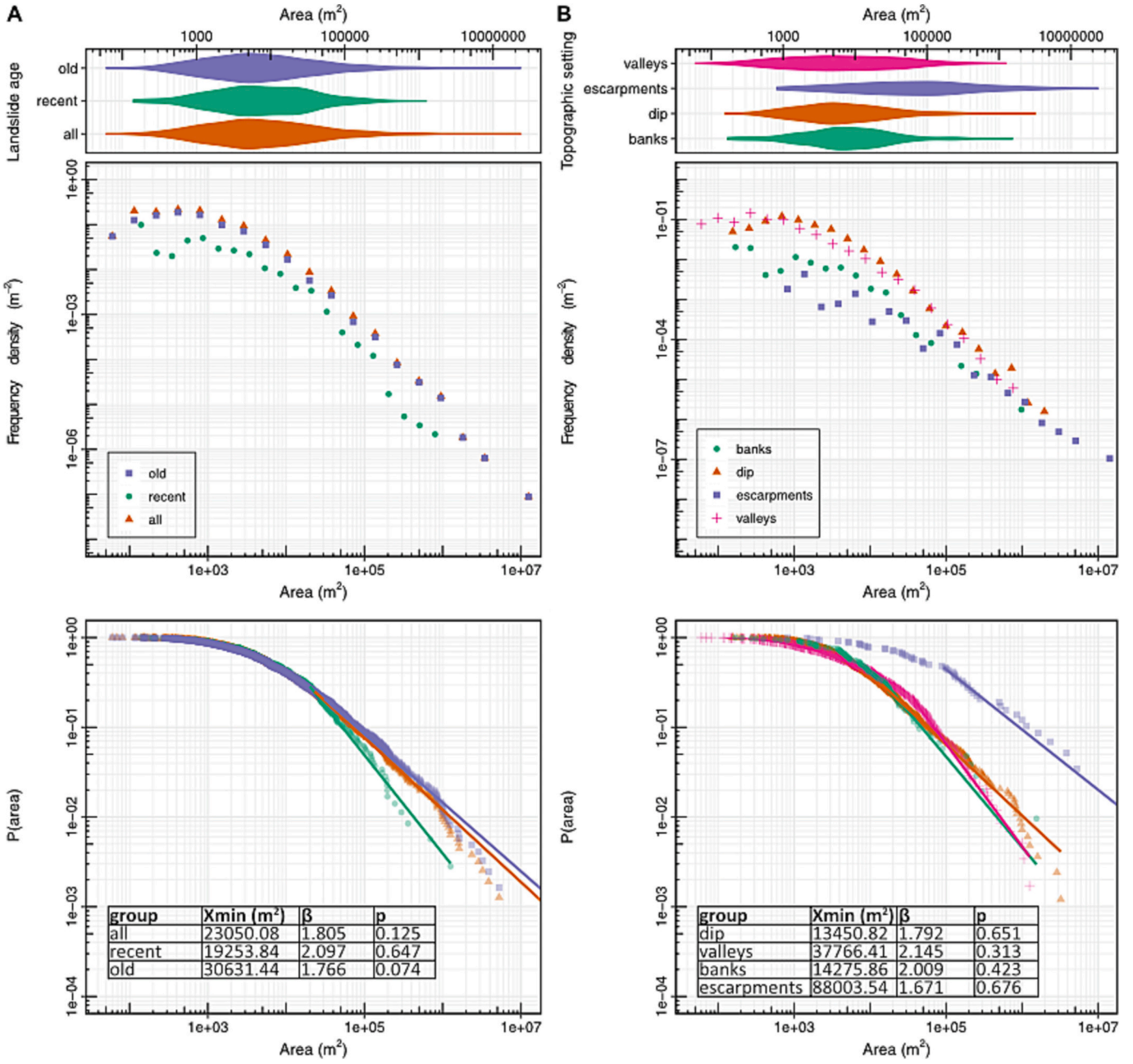

Fig. 4. Frequency-area statistics of inventoried landslides. The upper panels display violin plots of landslide size distribution, the middle panels show frequency-area distributions of landslides, and the lower panels depict cumulative density functions of landslide size, along with their maximum likelihood power-law fits. A. Landslide types categorized based on their relative age. B. Landslide types categorized based on topographic settings.

common type, accounting for 93 % (Table 1; Fig. 3), with planar/slab slides being the dominant subtype (39 %), followed by undifferentiated slides (24 %), shallow (debris) slides (20 %), and rotational slides (10 %). Flows, especially earth flows, are represented in only 6 % of cases, exclusively in the western and highest part of the study area (Fig. 3d). A small category (<1 %) is comprised of slope deformations (as defined by Hungr et al., 2014), involving usually complex deep-seated failures with some contribution of spreading and large, short-travelled rotational slides (Fig. 3c). Approximately a quarter of the landslides exhibit signs of recent activity (Fig. 3a), and around 3 % have been active since 2009 (Fig. 2d).

The landslides exhibit a highly clustered pattern, with two major hotspots: 1) the western part of the area, particularly in valleys incising the hanging wall of the Kura thrust, and 2) the vicinity of the Mingachevir Reservoir, with a significant concentration above its southern bank (Fig. 2c). These clusters account for approximately 60 % of all mapped landslides within the area, representing about one-tenth of the Kura fold-and-thrust belt. Recent landslides form spatially similar clusters to the overall dataset (Fig. 2d), and approximately half of the landslides that originated or were reactivated since 2009 are situated along the anticlines surrounding the Mingachevir Reservoir. The largest landslides (top 10 %) are distributed fairly evenly throughout the study area, aside from the mentioned clusters. In certain areas, such as the northern escarpment above the Alazani basin, they occur in isolation and are not accompanied by smaller landslides.

The size of the landslides varies significantly, spanning six orders of magnitude. The smallest shallow slides are <100 m^2, while the largest landslide covers an area of 24 km^2 (Fig. 3f). The frequency-area statistics

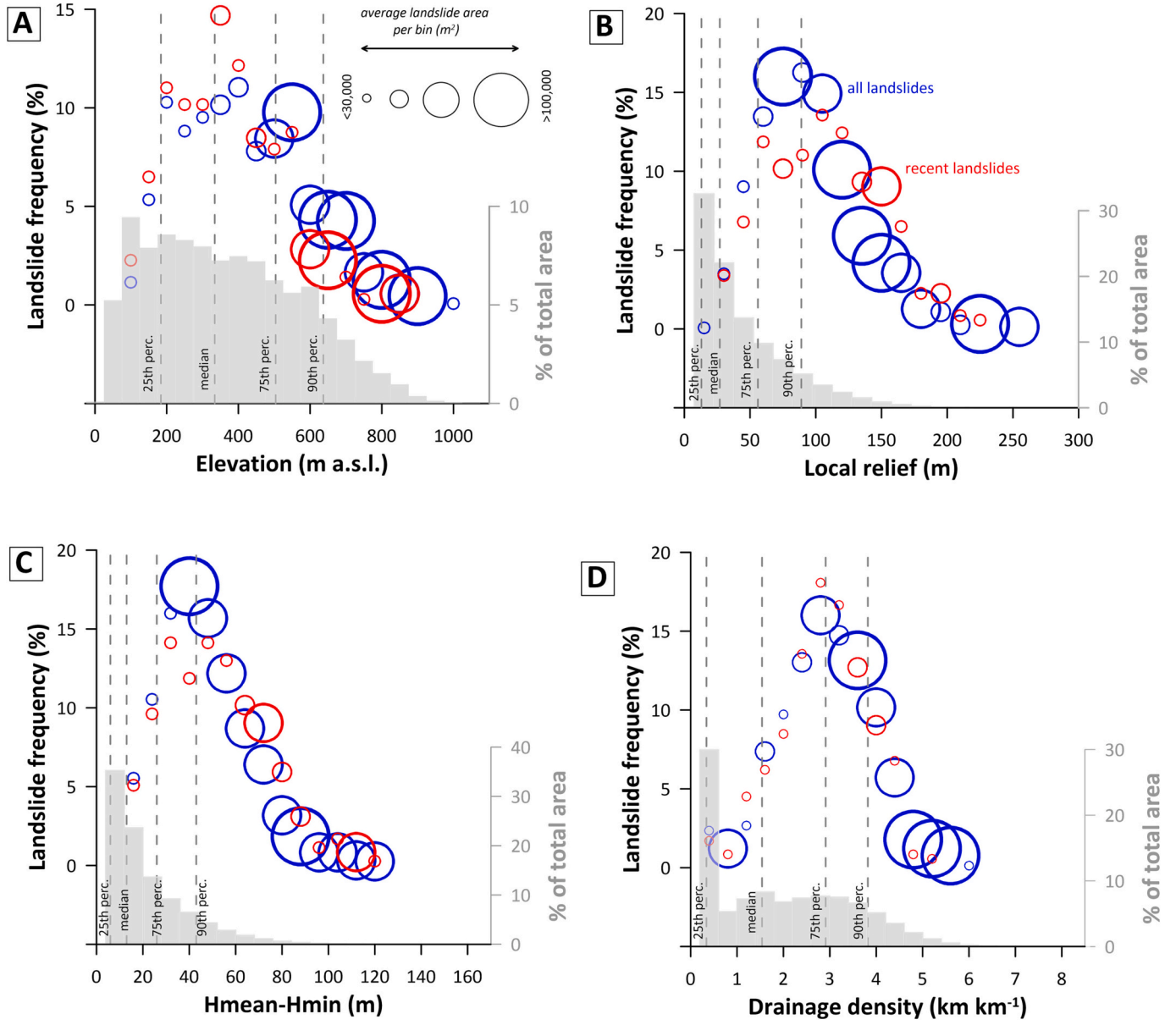

Fig. 5. Plot showing frequency of landslides and the average landslide size across different bins of topographic metrics. The data is presented separately for the entire landslide dataset and the subset of recent landslides. Grey bars show fraction of total landscape area. A. Landslide distribution based on elevation. B. Landslide distribution based on local relief. C. Landslide distribution based on the difference between the maximum (H_{max}) and minimum (H_{min}) altitude. D. Landslide distribution based on drainage density.

(Fig. 4a) follow a power law distribution, with parameters similar to other published regional landslide inventories, which typically have a range of power-law exponent β between 1.4 and 3.5 (Van Den Eeckhaut et al., 2007; Tebbens, 2020). However, the subset of recent landslides exhibits a higher power law exponent (β = 2.097), indicating a higher proportion of small landslides within this subset. On the other hand, the subset of old landslides demonstrates a lower β value (1.766), likely due to the removal of smaller landslides from the landscape as a result of erosion and anthropogenic activity (Fig. 3e).

4.2. Topographic distribution of landslides

Approximately half of the mapped landslides are situated on the dip slopes of folds, while more than a third are found in deeply incised valleys (Fig. 2b). The dip slopes along the flanks of anticlines produce planar/slab slides, which are the most common type of landslides in the area. These slides typically affect downslope-dipping conglomerates or other stronger lithologies that overlie softer argillaceous beds (Fig. 3a, b). A very small fraction of landslides is observed on undercut banks along larger laterally migrating rivers (7 %), as well as on escarpments (4 %) representing the slopes of thrusts and anaclinal slopes of isoclinal ridges according to Cruden and Hu (1999). The proportion of all landslides and recent landslides is generally similar across different topographic settings, with a slightly higher fraction of recent landslides observed on undercut banks (Fig. 2b). However, despite being the least frequent, landslides on escarpments exhibit the lowest β power law coefficient (1.671) in contrast to incised valleys with β = 2.145, indicating that this group, along with dip slopes (β = 1.792), contributes significantly to large landslides (Fig. 4b).

The distribution of landslides is significantly influenced by topographic metrics that approximate steepness and terrain dissection. According to Fig. 5, except for elevation, which exhibits the highest concentration of landslides around the median value, the majority of landslides are situated above the 75th regional percentile for local relief,

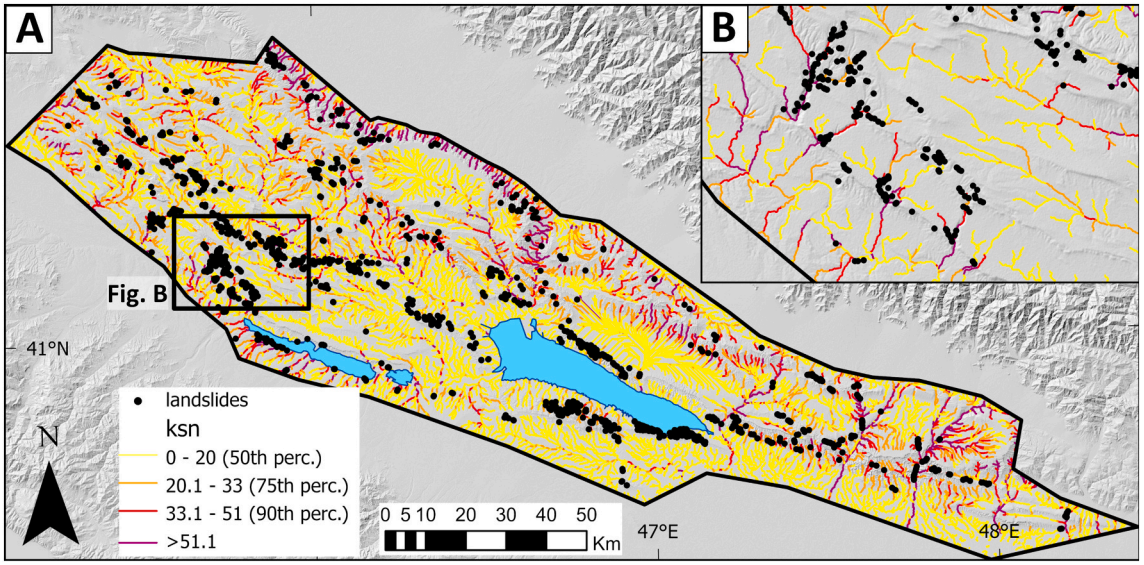

Fig. 6. Distribution of landslides and k_{sn} values. A. The entire territory of the Kura fold-and-thrust belt. B. Cutout from the k_{sn} index map illustrating the distribution of landslides in the western section of the Kura fold-and-thrust belt. Notably, the landslides are primarily concentrated within the valleys of channels exhibiting the steepest gradients, which correspond to the upper quartile of k_{sn} values in the entire Kura fold-and-thrust belt.

H_{mean}-H_{min}, and drainage density. In all the analyzed parameters, the largest landslides are consistently located exclusively above the 90th percentile, typically covering a very small portion of the landscape (Fig. 5).

Recent landslides and those that have taken place since 2009 are situated in steeper terrain compared to the entire landslide dataset (Table 1). Connected to this is also the distribution of landslides in relation to k_{sn} values, which serve as indicators of the steepness of the valley floor. Almost three-quarters of the landslides that occur on valley slopes (i.e., incised valleys and undercut banks in Fig. 2b) are concentrated within a buffer zone of one kilometer around valley floors with k_{sn} values surpassing the regional 75th percentile ($k_{sn} = 33$; Fig. 6).

4.3. Geological distribution of landslides

The size of landslides does not show significant differences among the individual geological units, although slightly larger landslides tend to occur in Pliocene and Miocene sediments (Fig. 7).

The majority of landslides are found on sediments from the Early Pleistocene Apsheron stage, followed by undifferentiated Quaternary sediments, Miocene Sarmatian, and Pliocene Akchagyl stages (Fig. 8). However, the higher percentage of landslides in undifferentiated Quaternary sediments is primarily due to the larger area coverage of this unit in the study area. Sarmatian beds and Akchagyl sediments exhibit the highest density of landslides, covering approximately 3.3 % and 2 % of the area of these geological units, respectively. The distribution of active landslides follows a similar pattern to the entire dataset, indicating a comparable susceptibility to landslides across the different geological units (Fig. 8).

The correlation between the size of individual landslides and their distance from thrust faults is weak, though nearly three-quarters of the landslides are concentrated within a 5-km radius of thrust faults. Furthermore, in terms of the total landslide area, over 50 % of it is located within one kilometer of thrust faults (Fig. 9). The 10,000 random points generated outside the landslide area display a more uniform distribution in terms of their distance from thrust faults. Additionally, the median distance of random points from faults is significantly higher ($p < 0.001$) compared to that of landslides (Fig. 9).

4.4. PCA analysis

Five principal components (PC1–PC5) have eigenvalues greater than one, explaining 84 % of the total multivariate space (Table 2). PC1–PC3 (Fig. 10) account for 71 % of the dataset's information. PC1 explains approximately 35 % of the data's variability, as shown in the PCA1 x PC2 biplot (Fig. 10). The biplot reveals two distinct clusters: one related to topographic steepness (H_{mean}-H_{min}, LR, and SL; refer to Table 2 for an explanation of abbreviations) with the highest PC1 loadings, and the other related to elevation and climate (RAIN, ELEV, and WET). The colour-coded PCA scores, depicting landslide coverage (%), indicate an increase in landslide density with terrain steepness, high elevation, and a wet climate. This trend is consistent in the PC1 x PC3 biplot (Fig. 10). Qu has a moderate positive loading on PC1 and is inversely correlated with the mentioned characteristics, negatively influencing landslide occurrence. FD and Hint have low negative loadings on PC1, indicating weak influence on landslide distribution. Among the geological units, Tak has the highest negative loading on PC1, while Qap, STD-SL, SL, and LR have the highest positive loadings on PC2.

5. Discussion

5.1. Why so few landslides?

Landslides cover approximately 0.8 % of the eastern part of the Kura fold-and-thrust belt. Even after excluding all basins and flat valley floors, the percentage of landslides per area remains <1 %. This percentage is comparable to tectonically stable Paleozoic mountains composed of strong crystalline rocks, such as the British Islands (Jarman and Harrison, 2019), but lower than what is observed in young Cenozoic mountain belts. In these mountain belts, landslides typically cover >1 % of the landscape. For example, landslides cover approximately 2 % in the Southern Alps of New Zealand (Allen et al., 2011), 5.6 % in the European Alps (Crosta et al., 2013), 4 % of the Armenian part of the Lesser Caucasus (Matossian et al., 2020), and 1.1 % in the Southern Carpathians (Gunnell et al., 2022). However, in the examples mentioned, the percentages of landslide coverage represent only minimum values as they only consider the distribution of rock-slope failures, neglecting shallow/debris slides and flows. In areas composed of relatively soft sedimentary rocks (e.g. flysch), landslide coverage can exceed 5 % (Pánek et al.,

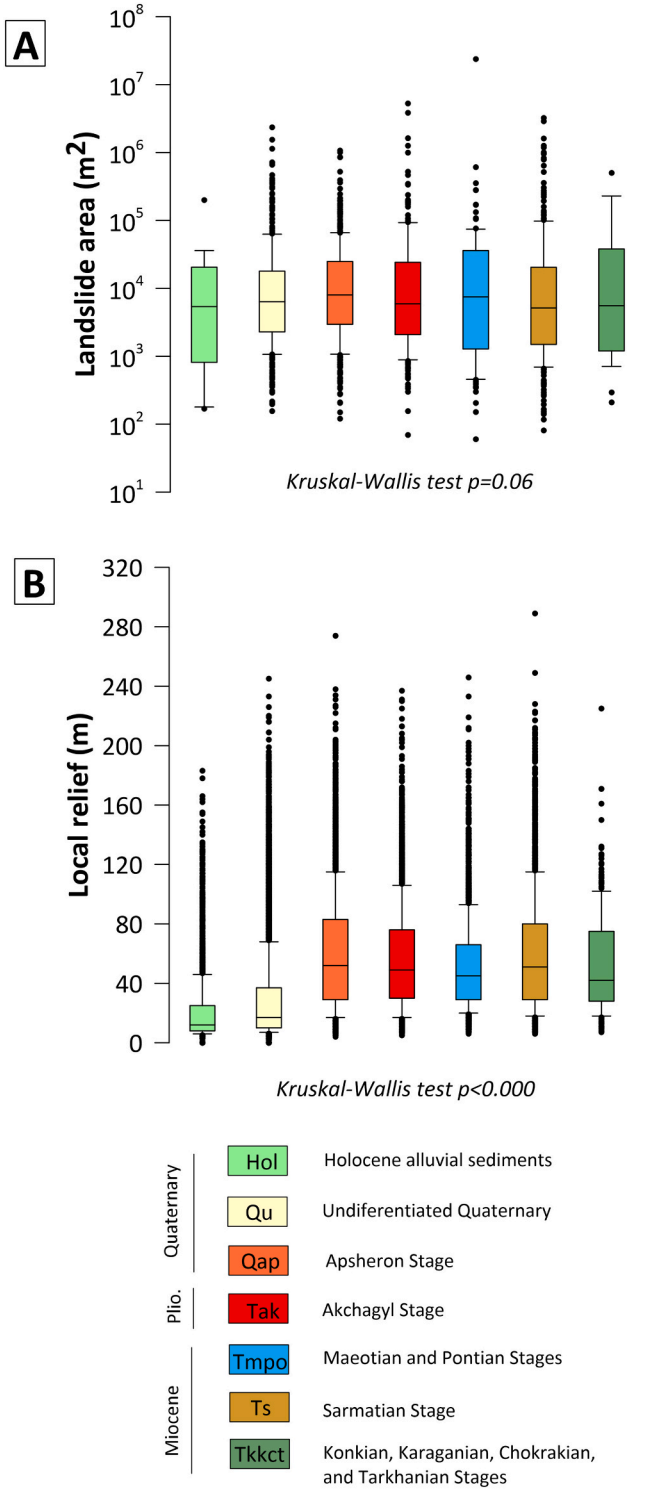

Fig. 7. Size of landslides (A) and mean local relief (B) of the main geological units constituting the Kura fold-and-thrust belt are depicted. The boxes represent quartiles, with whiskers extending to the 90th and 10th percentiles. The medians are indicated by center lines, and outliers are marked by black points. The *p*-value indicates the significance level based on the Kruskal-Wallis test.

2019). Furthermore, even in tectonically inactive low-gradient landscapes, landslide coverage often exceeds 1 % of the area (Van Den Eeckhaut et al., 2007). However, it should be emphasized that all mentioned landslide inventories are from climatically wet regions. Although the actual number of mapped landslides in the Kura fold-and-thrust belt may be affected by incomplete inventory (specially of small landslides; Tanyaş et al., 2019), partial forest coverage in NW, or poor satellite imagery in some areas, the region appears to have fewer morphologically detectable landslides than expected given the presence of landslide-prone sediments and significant tectonic activity.

The scarcity of landslides in the Kura fold-and-thrust belt can be attributed to several factors, including easily erodible sediments, semi-arid climate, absence of steep and high slopes, and human activities. Paradoxically, the region's young tectonic nature and relatively gentle slopes in specific folds may explain the infrequent landslides, as these folds are not yet fully developed and lack steep limbs (Hilley and Arrowsmith, 2008). Additionally, the predominantly sandy and loamy sediments in the area likely lead to rapid removal of small landslide features through erosion and diffusive hillslope processes (Fernandes and Dietrich, 1997). Agricultural activities have also reshaped or altered remnants of original landslides in many areas (Fig. 3e). A similar pattern was observed in the Outer Western Carpathians (Czechia), where anthropogenic removal of smaller landslides resulted in a relatively higher contribution of medium and large landslides and a lower power-law exponent β in cultivated landscapes compared to forested geomorphic units (Pánek et al., 2019).

5.2. *Landslide clustering: an interpretation*

Despite the relatively low overall frequency of landslides in the Kura fold-and-thrust belt, their distribution exhibits significant clustering (Fig. 2). In certain polygons generated for PCA, landslide coverage can exceed 20 % of the area (Fig. 10). In essence, landslides in the study area primarily occur in areas characterized by high elevation, steep slopes, and rugged terrain (Figs. 5 and 10). The topographic distribution of landslides and PCA results indicate that landslides are mainly influenced by the overall gradient of the topography (LR, SL, STD-SL variables), the depth of terrain dissection below the regional base level (H_{mean}-H_{min} variable), and relatively high rainfall (RAIN and WET variables). While the majority of the area receives <500 mm/year of rainfall, this amount can still be sufficient to trigger landslides in vegetation-free landscapes, especially on steep slopes close to the threshold angle (Moreiras and Sepúlveda, 2022). The dominance of geological/lithological units appears to have little influence (Fig. 10); however, detailed variations in lithology affecting the local distribution of landslides cannot be assessed due to the absence of high-resolution geological maps.

Furthermore, when considering the largest landslides, they tend to concentrate in the top few percent of the most exposed topography. Compared to landslide distribution in mountainous areas (e.g., Pánek et al., 2019), it seems that in a low-gradient terrain like the Kura fold-and-thrust belt, topography with limited maximum (and local relative) elevation plays a more pronounced role as a control factor for landslides. Landslides only occur in the “most extreme” relief of the area, while large areas remain completely free of landslides (Fig. 2). These conditions are particularly found in deeply-incised valleys that cut through the hanging walls of active thrusts and anticlines with steep flanks, many of which were identified as actively growing by Forte et al. (2010).

One of the most pronounced clusters of recent landslides is located on growing anticlines (Forte et al., 2010) along the banks of Mingachevir Reservoir (Fig. 2). The largest landslide cluster in this area is located on the Boz Dag anticline along the southern shore of the Mingachevir Reservoir (Fig. 11), where more than a third of the landslides are classified as recent (see e.g., Kotyuzhan and Molokov, 1990). As depicted in Fig. 11a, the density of landslides on the Boz Dag anticline increases from both plunging noses of the anticline towards its central part. Although some landslides along the northern flank of the anticline may have originated due to groundwater rise related to the filling of the Mingachevir Reservoir in 1959 (Kotyuzhan and Molokov, 1990; Bairamov et al., 1992; Yetirmishli et al., 2018; Islamova et al., 2019), the distribution of landslides on both flanks of the anticline is clearly controlled by the local slope steepness and the dip of the beds. Landslides are completely absent on both low plunging noses of the anticline,

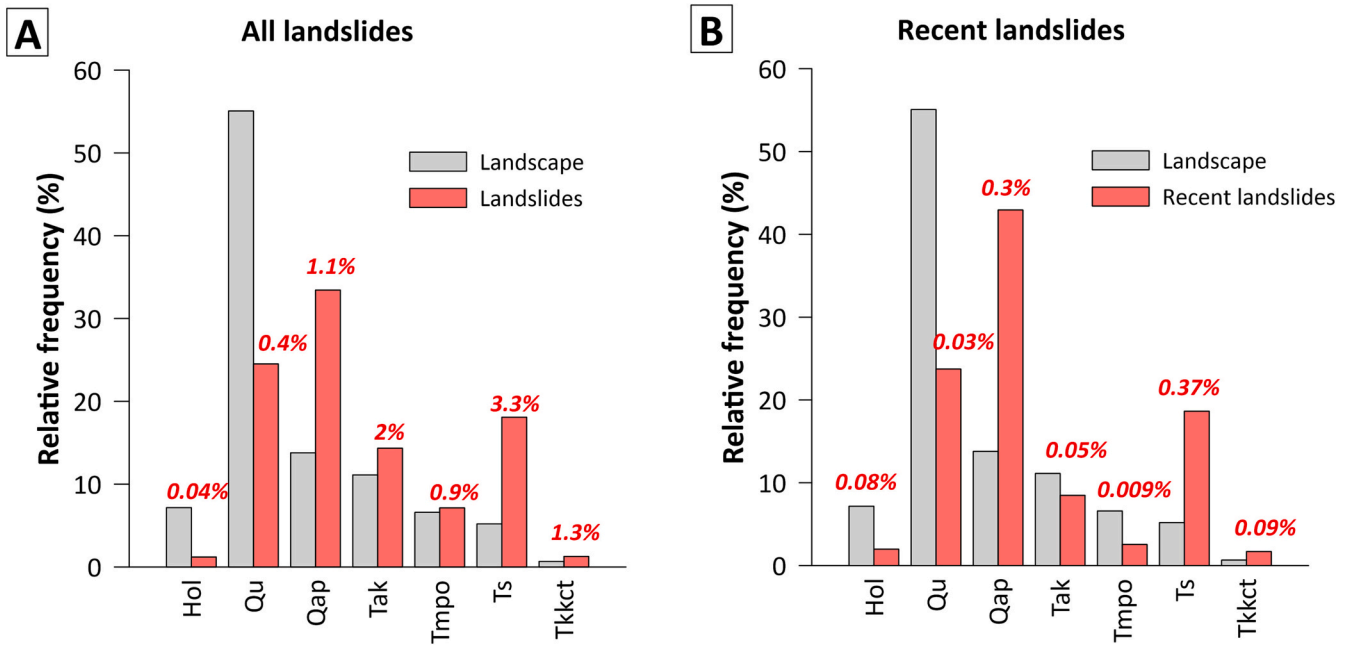

Fig. 8. Landslide frequency in individual geological units (for abbreviations of geological units see Fig. 7). The grey histogram represents the percentage of landscape covered by each individual geological unit in the total area. The red numbers displayed above the bars indicate the percentage of the area covered by landslides within a particular geological unit. (For interpretation of the references to colour in this figure legend, the reader is referred to the web version of this article.)

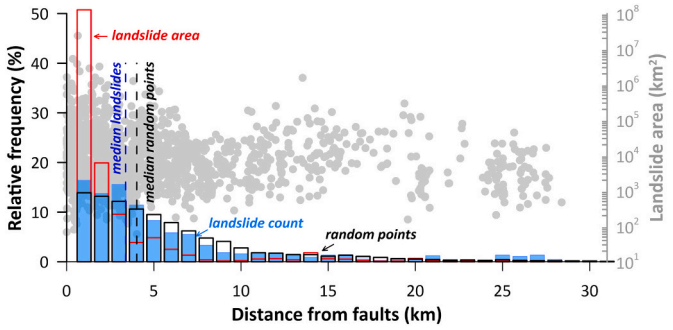

Fig. 9. The frequency and size of landslides as a function of the distance from thrust faults, in contrast to the distance of randomly generated points from thrust faults. The median distance of landslides is greater than that of random points, indicating a tendency for landslides to cluster near thrust faults.

and their occurrence is strictly confined to the highest central segment where the average dip of the beds exceeds 10° (Fig. 11b). This demonstrates that, similarly to the findings made by Delchiaro et al. (2023), landslides begin to develop when the anticline reaches a certain height, and the steepness of its limbs surpasses the friction angle of the material building the anticline.

The second typical setting of landslide clustering is observed in the valleys that cut across the hanging walls of active thrusts (Fig. 12). In such cases, landslides can occur even during the initial stage of anticline growth above the thrust, before the flanks have reached the threshold angle of slope failure. For instance, in the western part of the area along the Kura thrust, the left tributaries of the Kura River have formed deep valleys on the hanging wall, which are nearly completely affected by landslides. This is notable despite the fact that the backlimb of the growing anticline only reaches an inclination ~5–10° (Fig. 12a). The valleys are currently experiencing transient incision in response to ongoing uplift of the hanging wall of the Kura thrust. In a manner similar to that described by Harkins et al. (2007), Kirby et al. (2007), and Miller et al. (2012), this transitional incision is marked by the existence of stream knickpoints and the persistence of hanging valleys that cannot

Table 2
Results of the PCA.

Principal component	Main variables of principal component (component loadings)*	Eigenvalue	Explained variance	Cumulative variance
1	H_{mean}-H_{min} (−0.81), LR (−0.80), SL (−0.75), RAIN (−0.72), ELEV (−0.69), WET (−0.68), STD-SL (−0.66), K_{sn} (−0.66), DD (−0.63), Tak (−0.61), Qu (0.52), Tmpo (−0.45)	5.6	34.7	34.7
2	Qap (0.79), STD-SL (0.68), WET (−0.67), SL (0.63), ELEV (−0.61), RAIN (−0.57), LR (0.55), H_{mean}-H_{min} (0.51), Tak (−0.43)	3.7	23.3	58.0
3	Qu (−0.74), Hint (−0.65), DD (0.46), Ksn (−0.45), Tmpo (0.44), Ts (0.41)	2.0	12.6	70.6
4	Ts (−0.75), FD (−0.58)	1.1	7.1	77.7
5	FD (0.68), Ts (−0.43)	1.0	6.4	84.1

* Abbreviations used for variables entering the PCA: DD (mean drainage density), ELEV (mean elevation), FD (fault density), Hint (mean hypsometric integral), H_{mean}-H_{min} (difference between mean and minimum altitude), K_{sn} (mean normalized channel steepness index), LR (mean local relief), RAIN (mean annual precipitation), Qu (coverage by Quaternary undifferentiated deposits), Qap (coverage by Early Pleistocene Apsheron Unit), SL (mean slope), STD-SL (mean standard deviation of slope), WET (mean precipitation of wettest month), Tak (coverage by Pliocene Akchagyl Unit), Tmpo (coverage by Miocene Meaotian and Pontian Units), Ts (coverage by Miocene Sarmatian Unit).

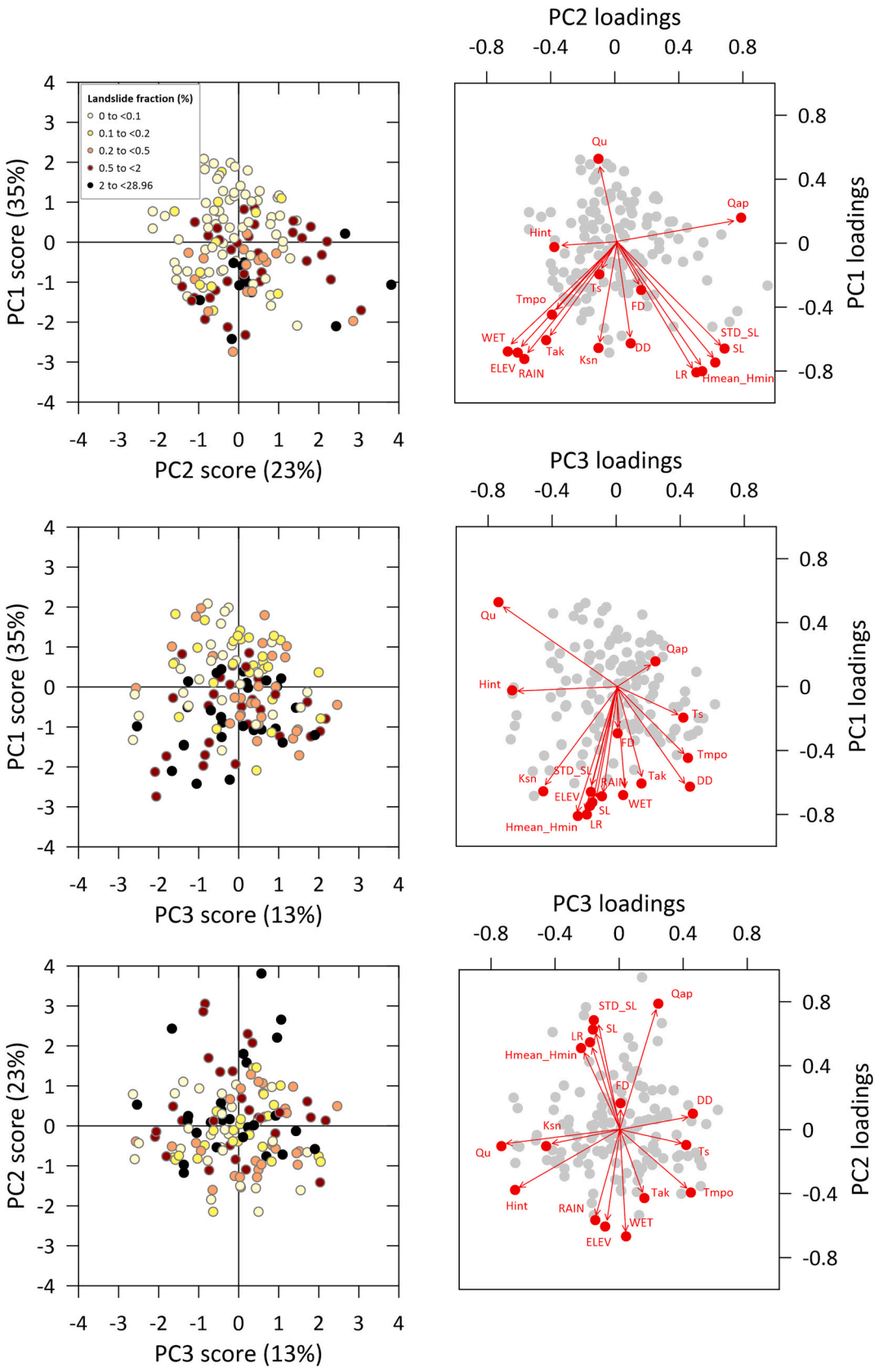

Fig. 10. PCA results showing principal component scores and loadings for the first three principal components (PC1–PC3). For labels abbreviations see Table 2.

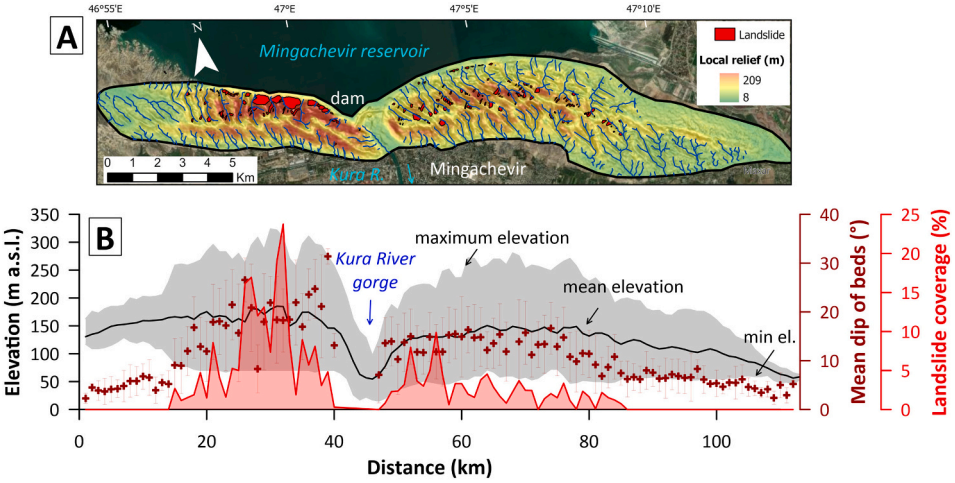

Fig. 11. Landslide distribution on the Boz Dag anticline, located on the southern shore of the Mingachevir reservoir. A. The distribution of landslides versus local relief. B. A swath profile along the axis of the anticline displaying the topography (maximum, mean, and minimum elevation), the average dip of the strata, and the extent of landslide coverage (%). The dip of the strata was estimated from the gradient of dip slopes; only those parts of the slopes that clearly conform to the dip of the beds, as indicated by satellite images, were selected for measurement. All parameters pertain to 250-meter-wide strips.

deepen at the same rate as the main valleys (see Fig. 12b, c). The steep hillslopes of the gorges are heavily affected by landslides, many of which are still active, and their size and frequency diminishes upstream from the thrust (Fig. 12d). While PCA analysis does not reveal fault density as a crucial factor for the overall distribution of landslides in the Kura fold-and-thrust belt (Fig. 10), the presence of uplifting hanging walls of thrusts, when incised by antecedent valleys, clearly governs the distribution of landslides in the study area.

5.3. Potential role of seismicity

In tectonically active areas, such as the Kura fold-and-thrust belt, seismicity is a key trigger for landslides (Keefer, 1984; Tibaldi et al., 1995; Fan et al., 2019; Görüm et al., 2014; Tanyaş and Lombardo, 2019; Tanyaş et al., 2019). Landslides induced by earthquakes resulting from the ongoing collision between the Arabian and Eurasian plates have been documented in surrounding regions, both in the Caucasus (Jibson et al., 1994; Matossian et al., 2020) and Anatolia (Görüm, 2019; Görüm et al., 2023). While earthquakes may have triggered landslides in the Kura fold-and-thrust belt in the past, the distribution of recently identified landslide clusters cannot be explained by seismic activity. This is evident from the overlapping clusters of old and recent landslides (Fig. 2c, d). In fact, landslides that occurred in the last few decades, including those after 2009 (Fig. 2d), were not triggered by seismicity due to the absence of strong earthquakes.

While some mapped landslides may have been caused by past seismicity, almost a millennium has passed since the last significant earthquake, the M~7 AD 1139 Ganja earthquake (Ismail-Zadeh et al., 2020). Consequently, many landslides, especially in actively incising valleys and on dip slopes on anticlinal limbs, have likely been triggered by other factors, such as heavy rainfall, river undercutting, or anthropogenic activities (Kotyuzhan and Molokov, 1990; Bairamov et al., 1992; Yetirmishli et al., 2018; Islamova et al., 2019). In other settings, such as fault escarpments distal to actively eroding rivers, we speculate that large, old landslides may have a seismic origin, whereas smaller landslides have been removed due to erosion or anthropogenic activities since the last earthquake. The remaining large landslides in the current landscape can be considered remnants of previously more extensive landslide populations that existed immediately after the past earthquake events. This interpretation is supported by the absence of smaller landslides accompanying the relatively large ones found on steep escarpments along the northern and southern boundaries of the area (Figs. 2c, d).

In any case, investigating the influence of seismicity on landslides in the Kura fold-and-thrust belt remains a topic for further research. For example, one question is whether moderate earthquakes with Mw ~ 5–6, which have occurred in the vicinity of the study area in the last century, may have reactivated some landslides.

5.4. Slope deformations along active thrusts

The frequency-area statistics show that landslides on fault escarpments tend to be relatively large in comparison to other topographic settings. This is supported by the lowest power law β coefficient among all topographic settings (Fig. 4b). A specific type of landslide that exclusively occurs along the outermost Kura frontal thrust at the margin of the area is characterized by massive slope deformations with grabens, open cracks, and counter-slope scarps (Fig. 13). These features resemble deep-seated gravitational slope deformations (DSGSDs) commonly found in bedrock (Agliardi et al., 2001). In our area, characterized by unconsolidated or poorly indurated sediments, we refer to these landslides simply as slope deformations (Hungr et al., 2014). In some cases, they exhibit characteristics of large, short-travelled rotational slides and spreads (Fig. 13d), with barely perceptible scarps that extend hundreds of meters into the plateaus above the thrust scarps (Fig. 13a, b, e).

As indicated by studies conducted in other tectonically and seismically active regions (e.g., Algeria or Italy), slope deformations characterized by spreads and crestal grabens are frequently observed in overthrust blocks, particularly when composed of weak and/or unconsolidated sediments (Dramis and Sorriso-Valvo, 1994). These slope deformations are typically initiated by the genesis of crestal coseismic ruptures, which occur orthogonal or oblique to the principal shortening direction (Phillips and Meghraoui, 1983). Subsequently, they progress as gravity-driven spreads, sagging, and toppling of elevated hanging walls of thrusts (Dramis and Sorriso-Valvo, 1994). Aligned with these observations, the mapped slope deformations could suggest a combination of ongoing strain on the Kura thrust and potential coseismic deformations associated with historical earthquakes. Field inspections of slope deformation sites indicate a notable degradation of the scarps (Fig. 13 b, e), implying a substantial time interval since the occurrence of the last significant earthquake, possibly the AD 1139 Ganja earthquake or an earlier event.

5.5. Landslides in the growing fold-and-thrust belts

Based on observations of the distribution of landslides on folds at

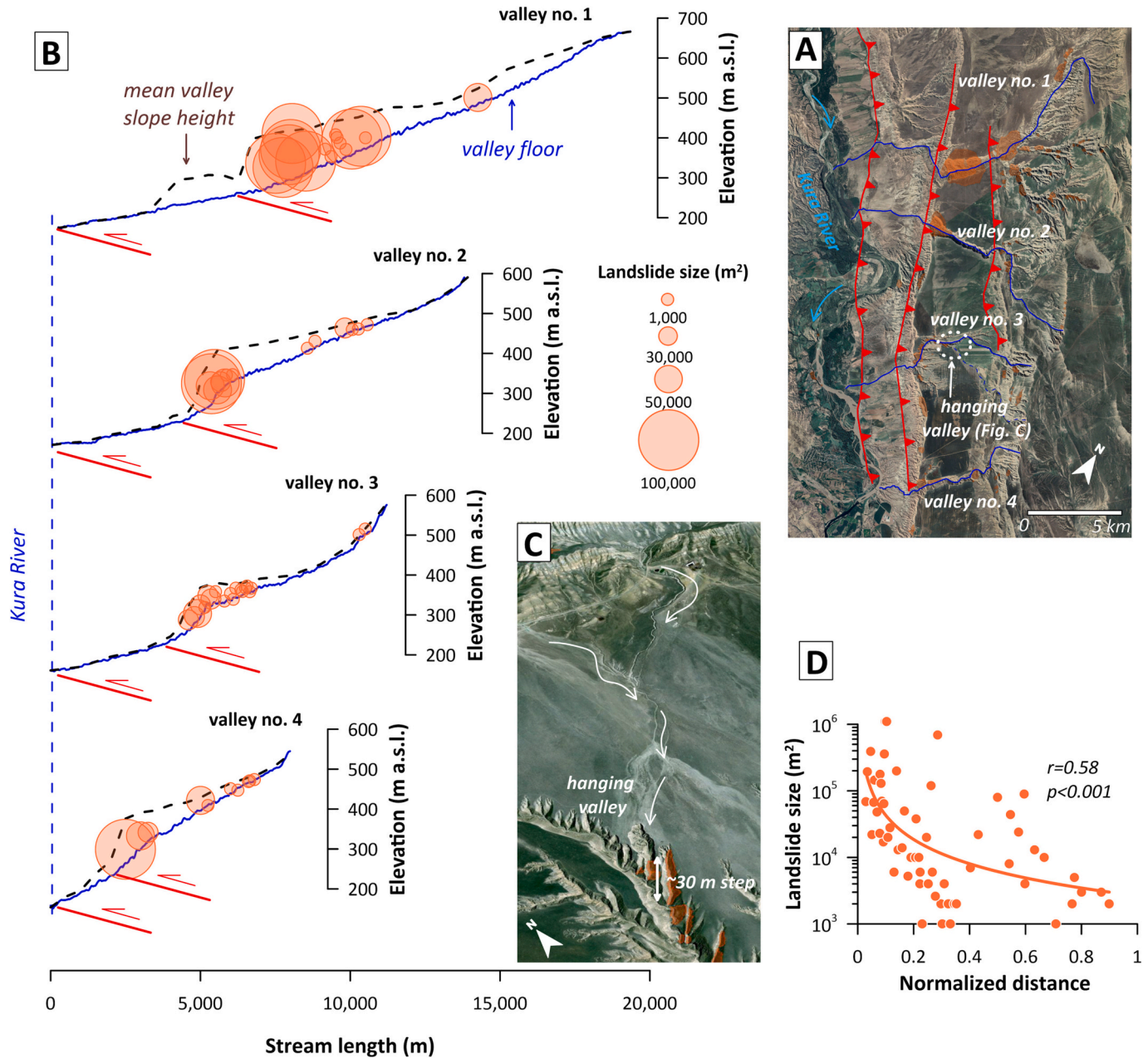

Fig. 12. Landslides in the valleys incising through Kura thrust hanging wall in the western part of the study area (for location see Fig. 2a). A. Distribution of landslides and footprints of thrust faults displayed on a Google Earth™ image. B. Longitudinal profiles of valleys intersecting the Kura thrust, with dashed lines indicating valley depth (average height of opposing right and left valley slopes measured at 500 m intervals). Note the pronounced knickpoints upstream of the thrust faults, which coincide with the distribution of the largest landslides and deepest sections of the valley. C. Hanging valley as evidence of the transient incision of major valleys in response to recent uplift of the hanging wall. D. Plot showing the relationship between landslide size and the upstream distance from the point where valleys crosscut the thrust escarpment.

various stages of development, the Kura fold-and-thrust belt could potentially serve as a representative region for understanding the temporal evolution of landslide patterns in belts composed of weak sediments without a core formed by strong rocks (see e.g., Burbank et al., 1999).

For landslides to occur, the fold-and-thrust belt must reach a certain stage of development (Delchiaro et al., 2023). This involves the presence of folds with steep flanks that concentrate enough topographic stresses, as well as the uplift of the hanging wall causing the formation of deeply incised valleys. The western part of the area, as noted by Forte et al. (2013), experienced greater contraction and uplift, leading to the development of higher and steeper topography and deeper exposure of geological structures (Fig. 1). The formation of folds with steep flanks created unstable conditions, where the dip slopes exceeded the friction angle of local sediments, resulting in numerous planar slides on the limbs of anticlines. On the other hand, in the eastern part of the area, which contains early-stage or less uplifted anticlines, many of them lack sufficiently steep flanks to initiate landslides (Mosar et al., 2010; Forte et al., 2010, 2013). The distinction in landslide development between open (low gradient) and tight (steep) anticlines is attributed to headward erosion towards the fold axes. In the case of tight anticlines, the progressive extension of the valley network potentially leads to an emergence of increasing number of dip slopes in the center of the anticline that are susceptible to planar/slab landslides (Cruden and Hu, 1999). This results in substantial clusters of landslides extending across a significant portion of the anticline (Fig. 11). Conversely, in the case of

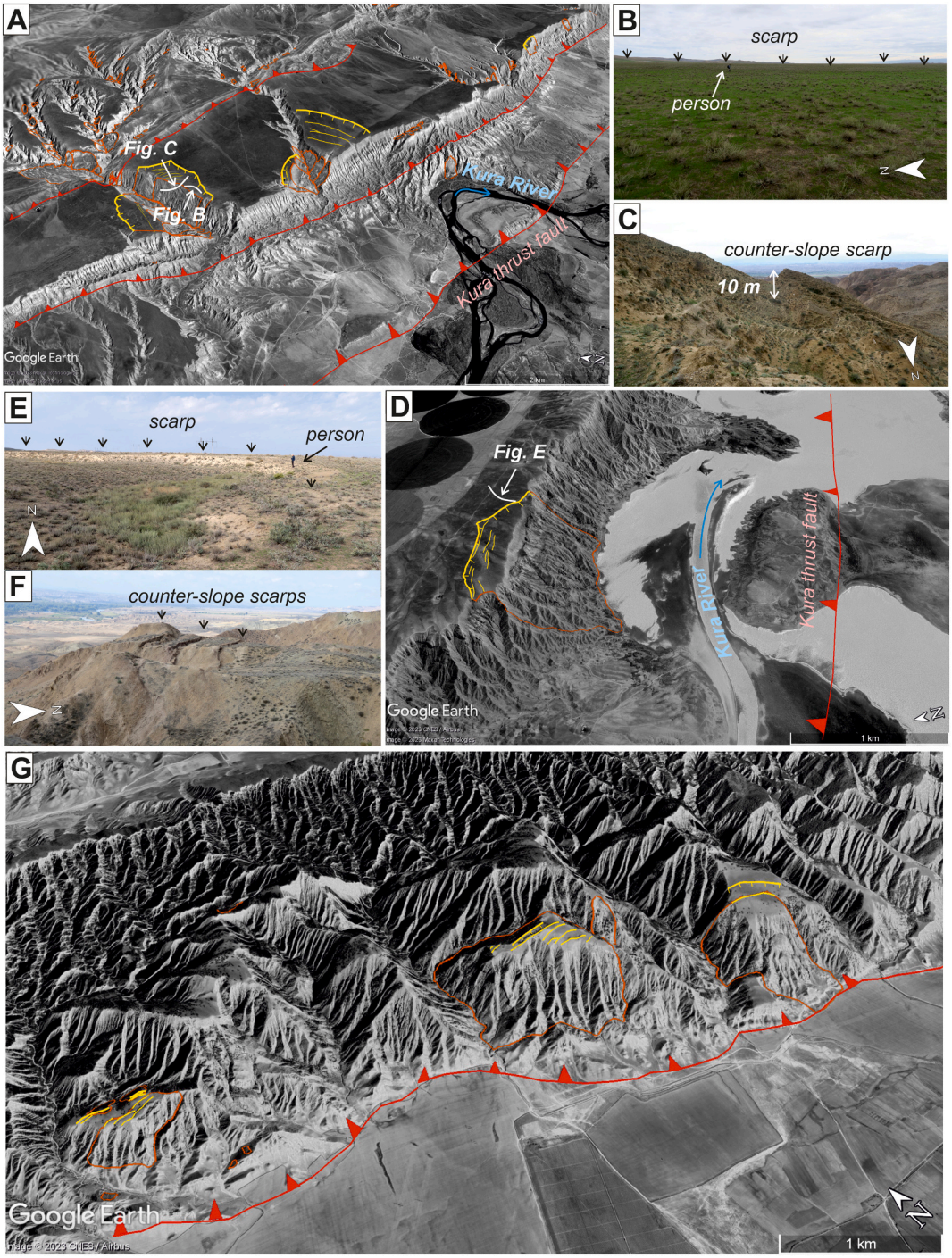

Fig. 13. Slope deformations affecting hanging walls and deeply incised valleys upstream of active thrusts. Scarps and trenches of slope deformations are indicated by yellow lines. A. Slope deformations situated at the outlets of hanging wall valleys to the Kura River valley in the western part of the study area. B. Less than 1-meter-high subdued scarp protruding over 300 m into the plateau, located above a deeply incised valley. C. Counter-slope scarps suggest active toppling deformation above the incising valley. D. Slope deformation above the western termination of the Shamkir Reservoir. The deformation consists of a massive, short-travelled rotational slide undercutting the plateau, with the presence of scarps and grabens. E. A subdued scarp forming the northern limit of the slope deformation. F. Counter-slope scarps suggest active toppling on the escarpment of the Kura thrust fault. G. Frequent slope deformations on the hanging wall of the Kura thrust, eastward from the Mingachevir reservoir. (For interpretation of the references to colour in this figure legend, the reader is referred to the web version of this article.)

gentle folds, unstable conditions occur primarily along major incising valleys. However, due to the insufficient dip of the beds, planar/slab slides are less common, resulting in a lower overall density of landslides within these folds. Our study shows, similar to findings from other landscapes dominated by isoclinal or folded structures (e.g., Pánek et al., 2019; Chigira et al., 2022; Delchiaro et al., 2023), that dip slopes represent hotspots of landslide activity and areas with increased landslide-related erosion (Cruz Nunes et al., 2015).

In summary, the distribution of landslides in propagating fold-and-thrust belts can be explained by the following evolutionary model (Fig. 14). Initially, during the early uplift of the hanging wall, the fold flanks are not steep enough to trigger landslides. Instead, landslides concentrate in incising valleys perpendicularly crossing the growing hanging walls. Short-travelled deep-seated slope deformations may

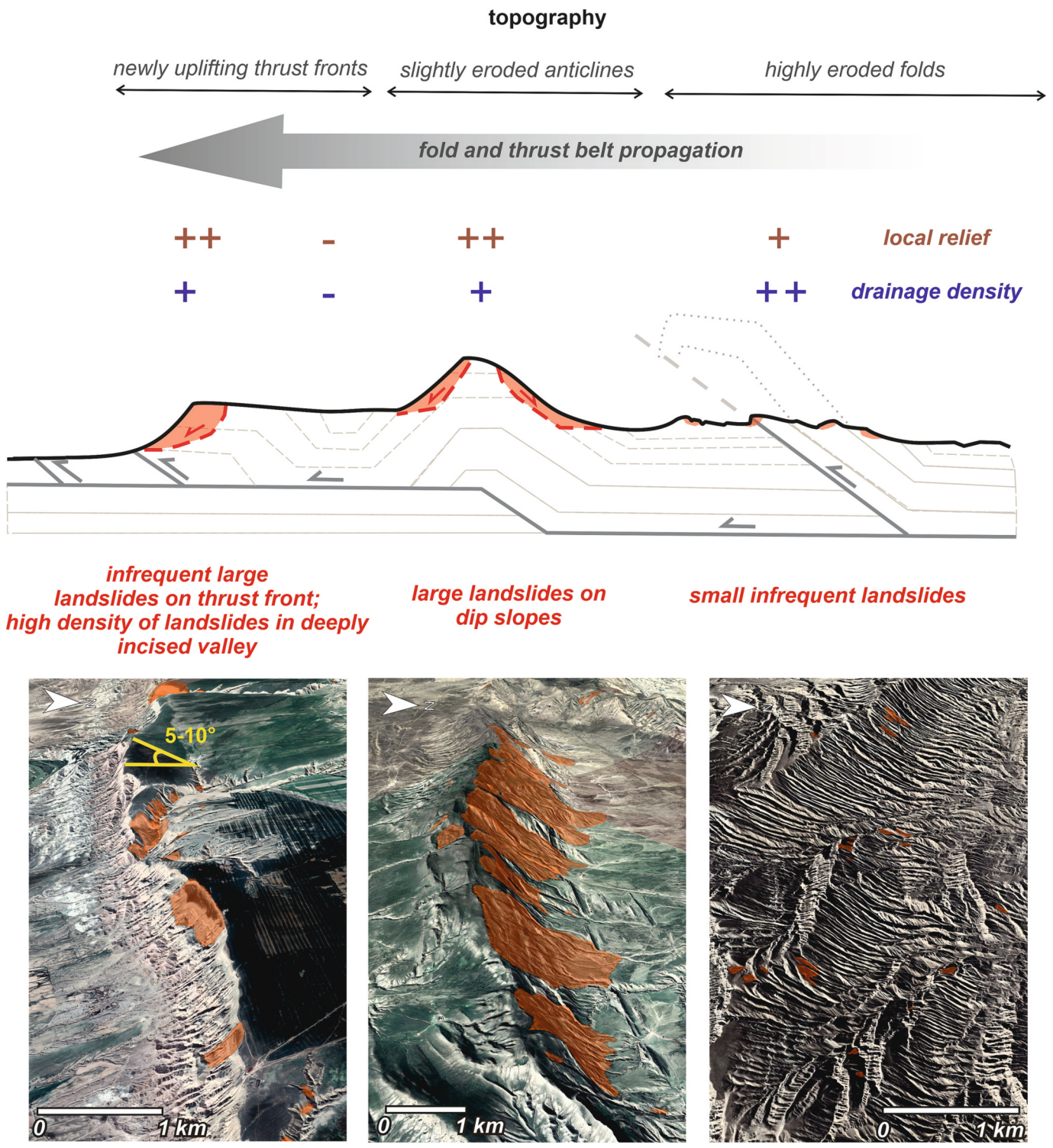

Fig. 14. Conceptual scheme illustrating the landslide patterns affecting a propagating fold-and-thrust belt. The left part of the scheme shows a newly emerged thrust scarp, the middle part depicts a steep-growing anticline, and the right part represents highly eroded and lowered folds. For a detailed description, please refer to the main text.

affect the emerging thrust scarps in specific areas (Fig. 14). This pattern is observed throughout the majority of the Kura thrust, particularly in its western and eastern sections (Fig. 2). As uplift progresses, landslides concentrate on the flanks of the anticlines and may occur even in the axial parts when headward erosion exposes dip slopes in older formations. If the fold flanks consist of stronger sediments such as conglomerates, sandstones, or limestones, they form persistent topographic elevations (e.g., hogbacks) and experience larger landslides. This condition is observed in the Mingachevir Reservoir area and the western portion of the Kura fold-and-thrust belt (Fig. 14).

In the final stage, as erosion and exhumation continue, the anticlines decrease in elevation, resulting in a reduced potential for landslides (Fig. 14). In the eastern part of the Kura fold-and-thrust belt, the Apsheron and Akchagyl sedimentary formations, which make up the

majority of anticlines, contain conglomerates and coarse sands in the upper part and more argillaceous sediments at the bottom of the sequences (Forte et al., 2014). The removal of stronger sediments has led to the development of badlands dominated by gully erosion, with only occasional large landslides occurring. While badlands can host numerous small shallow landslides, these often fall below the resolution level when mapped using satellite imagery.

While the model is applicable to the forward sequence of fold-and-thrust belts, questions persist about landslides in the backward sequence (along backthrusts) and in out-of-sequence deformations. In the study area, a northern backthrust-related scarp, with higher local relief than the most recent frontal Kura thrust scarp, suggests a more advanced stage of development. Unlike the frontal thrust, the backthrust-related scarp lacks incipient slope deformation but mainly showcases fully developed large landslides (Fig. 2c). Nevertheless, the relationship between landslide development and backthrust or out-of-sequence folds and thrusts should be clarified in the future with a better understanding of the absolute and relative chronology of these deformations.

6. Conclusion

We mapped nearly 1600 landslides across an area of over 13,000 km^2, encompassing the majority of the tectonically active Kura fold-and-thrust belt in the southeast of the Greater Caucasus. Because of the semiarid climate, the relatively smooth relief with limited elevation variation, and the absence of a major earthquake in the last 1000 years, the number of landslides is relatively low. Their distribution is highly concentrated, with significant clusters occurring in deeply incised valleys that intersect uplifting thrusts and on the steep flanks of anticlines. The largest cluster of active landslides is located along the southern shore of the Mingachevir water reservoir, which is a major energy infrastructure for Azerbaijan. In most other parts of the area, landslides are sporadic and show little current activity. These may be remnants of a past landslide population triggered by (pre)historic earthquakes that have been eroded or removed by human activity. Comparing the distribution of landslides on different folds reveals that newly emerging folds above thrust hanging-walls lack steep flanks prone to landslides. However, landslides concentrate in valleys crosscutting hanging-walls of thrusts where steep hillslopes are present. The continued growth of anticlines and increased strata dip contribute to an elevated frequency of landslides, as landslide-prone dip slopes form along the flanks and center of the anticlines. Conversely, ongoing erosion of the folds, particularly those outside the active front of the fold-and-thrust belt, leads to a reduction in anticline height and a decrease in landslide frequency. Further research should investigate the influence of lithologically complex sediments on landslide distribution and characteristics, identify potential paleoseismological signals in the spatial and temporal distribution of landslides in the Kura fold-and-thrust belt, and monitor large active landslides along the banks of the Mingachevir water reservoir.

Supplementary data to this article can be found online at https://doi.org/10.1016/j.geomorph.2024.109059.

CRediT authorship contribution statement

Tomáš Pánek: Conceptualization, Data curation, Formal analysis, Funding acquisition, Methodology, Writing – original draft, Writing – review & editing, Investigation. **Michal Březný:** Conceptualization, Data curation, Methodology, Writing – original draft, Writing – review & editing, Investigation. **Hans-Balder Havenith:** Investigation, Writing – original draft, Writing – review & editing. **Alessandro Tibaldi:** Conceptualization, Funding acquisition, Writing – original draft, Writing – review & editing.

Declaration of competing interest

The authors declare that they have no known competing financial interests or personal relationships that could have appeared to influence the work reported in this paper. We confirm that this submission contains original material that has been neither published elsewhere nor simultaneously submitted for consideration in any other journal. All the utilized data are properly cited in references.

Data availability

Data will be made available on request.

Acknowledgements

This study has been conducted in the framework of the 2022-2025 NATO project SPS G5907 “Prevention of Geo-Threats to Azerbaijan's Energy Independence”. We would like to acknowledge Fritz Schlunegger and anonymous reviewer for their careful reviews and valuable comments that improved the manuscript.

References

Agliardi, F., Crosta, G.B., Zanchi, A., 2001. Structural constrains on deep–seated slope deformations kinematics. Eng. Geol. 59, 83–102.
Alania, V., Chabukiani, A., Chagelishvili, R., Enukidze, O., Gogrichiani, K., Razmadze, A., Tsereteli, N., 2017. Growth structures, piggy-back basins and growth strata of the Georgian part of the Kura foreland fold-thrust belt: implications for late Alpine kinematic evolution. In Tectonic Evolution of the Eastern Black Sea and Caucasus (eds M Sosson, RA Stephenson and SA Adamia). Geol. Soc. Lond. Spec. Publ. 428, 171–185.
Allen, S.K., Cox, S.C., Owens, I.F., 2011. Rock avalanches and other landslides in the central Southern Alps of New Zealand: a regional study considering possible climate change impacts. Landslides 8, 33–48.
Bairamov, R.I., Veli-Zade, T.Y., Molokov, L.A., 1992. More on the landslide at Mingechaurskoye Reservoir. Gidrotekhnicheskoe Stroitel'stvo 4, 38–41.
Borsuk, A.M., Sholpo, V.N., 1983. Correlation of endogenous processes in the Alpine cycle of the Caucasus. In: Rast, N., Delany, F.M. (Eds.), Profiles of Orogenic Belts, Geodyn. Ser., vol. 10. AGU, Washington, D. C, pp. 97–143.
Bull, W.B., 2007. Tectonic Geomorphology of Mountains. A New Approach to Paleoseismology. Blackwell Publishing Ltd., Oxford, 316 p.
Burbank, D.W., McLean, J.K., Bullen, M.E., Abdrakhmatov, K.Y., Miller, M.M., 1999. Partitioning of intermontane basins by thrust-related folding. Tien Shan, Kyrgyzstan. Basin Res. 11, 75–92.
Chigira, M., Tsou, C.-Y., Higaki, D., Amatya, S.C., 2022. A series of rockslides and gravitational slope deformations aligned along the Kali Gandaki across the Nepal Himalaya. Geomorphology 400, 108098.
Clauset, A., Shalizi, C.R., Newman, M.E.J., 2009. Power-law distributions in empirical data. SIAM Rev. 51, 661–703.
Crosta, G., Frattini, P., Agliardi, F., 2013. Deep seated gravitational slope deformations in the European Alps. Tectonophysics 605, 13–33.
Cruden, D.M., Hu, X.Q., 1999. The shapes of some mountain peaks in the Canadian Rockies. Earth Surf. Process. Landf. 24, 1–13.
Cruden, D.M., Varnes, D.J., 1996. Landslide types and processes. In: Turner, A.K., Schuster, R.L. (Eds.), Landslides Investigation and Mitigation. Transportation Research Board, US National Research Council. Special Report 247, Washington, DC, pp. 36–75.
Cruz Nunes, F., Delunel, R., Schlunegger, F., Akçar, N., Kubik, P.W., 2015. Bedrock bedding, landsliding and erosional budgets in the central European Alps. Terra Nova 27, 370–378.
Delchiaro, M., Della Seta, M., Martino, S., Nozaem, R., Moumeni, M., 2023. Tectonic deformation and landscape evolution inducing mass rock creep driven landslides: the Loumar case-study (Zagros Fold and Thrust Belt, Iran). Tectonophysics 846, 229655.
Dramis, F., Sorriso-Valvo, M., 1994. Deep–seated gravitational slope deformations, related landslides and tectonics. Eng. Geol. 38, 231–243.
Fan, X., Scaringi, G., Korup, O., West, A.J., van Westen, C.J., Tanyaş, H., Hovius, N., Hales, T.C., Jibson, R.W., Allstadt, K.E., Zhang, L., Evans, S.G., Xu, C., Li, G., Pei, X., Xu, Q., Huang, R., 2019. Earthquake-induced chains of geologic hazards: patterns, mechanisms, and impacts. Rev. Geophys. 57, 421–503.
Fernandes, N.F., Dietrich, W.E., 1997. Hillslope evolution by diffusive processes: the time scale for equilibrium adjustments. Water Resour. Res. 33, 1307–1318.
Fick, S.E., Hijmans, R.J., 2017. WorldClim 2: new 1km spatial resolution climate surfaces for global land areas. Int. J. Climatol. 37, 4302–4315.
Forte, A.M., Cowgill, E., Bernardin, T., Kreylos, O., Hamann, B., 2010. Late Cenozoic deformation of the Kura fold-thrust belt, southern Greater Caucasus. Geol. Soc. Am. Bull. 122, 465–486.
Forte, A.M., Cowgill, E., Murtuzayev, I., Kangarli, T., Stoica, M., 2013. Structural geometries and magnitude of shortening in the eastern Kura fold-thrust belt,

Azerbaijan: implications for the development of the Greater Caucasus Mountains. Tectonics 32, 688–717.
Forte, A.M., Cowgill, E., Whipple, K.X., 2014. Transition from a singly vergent to doubly vergent wedge in a young orogen: the Greater Caucasus. Tectonics 33, 2077–2101.
Forte, A.M., Sumner, D.Y., Cowgill, E., Stoica, M., Murtuzayev, I., Kangarli, T., Elashvili, M., Godoladze, T., Javakhishvili, Z., 2015. Late Miocene to Pliocene stratigraphy of the Kura Basin, a subbasin of the South Caspian Basin: implications for the diachroneity of stage boundaries. Basin Res. 27, 247–271.
Gillespie, C.S., 2015. Fitting heavy tailed distributions: the poweRlaw package. J. Stat. Soft. 64 https://doi.org/10.18637/jss.v064.i02.
Görüm, T., 2019. Tectonic, topographic and rock-type influences on large landslides at the northern margin of the Anatolian Plateau. Landslides 16, 333–346.
Görüm, T., Korup, O., van Westen, C.J., van der Meijde, M., Xu, C., van der Meer, F.D., 2014. Why so few? Landslides triggered by the 2002 Denali earthquake, Alaska. Quat. Sci. Rev. 95, 80–94.
Görüm, T., Tanyaş, H., Karabacak, F., Yilmaz, A., Girgin, S., Allstadt, K.E., Süzen, M.L., Burgi, P., 2023. Preliminary documentation of coseismic ground failure triggered by the February 6, 2023 Türkiye earthquake sequence. Eng. Geol. 327, 107315.
Gunnell, Y., Blondeau, S., Jarman, D., 2022. Rock slope failure in the Southern Carpathians (Romania): Range-wide inventory and links with long-term mountain landscape evolution. Geomorphology 418, 108433.
Hammerstein, J.A., Di Cuia, R., Cottam, M.A., Zamora, G., Butler, R.W.H., 2020. Fold and thrust belts: structural style, evolution and exploration – an introduction. Geol. Soc. Lond. Spec. Publ. 490, 1–8.
Harkins, N., Kirby, E., Heimsath, A., Robinson, R., Reiser, U., 2007. Transient fluvial incision in the headwaters of the Yellow River, northeastern Tibet, China. J. Geophys. Res. Earth 112, 1–21.
Havenith, H.B., 2022. Recent earthquake-triggered landslide events in Central Asia, evidence of seismic landslides in the lesser caucasus and the carpathians. In: Towhata, I., Wang, G., Xu, Q., Massey, C. (Eds.), Coseismic Landslides, Phenomena, Long-term effects and Mitigation. Springer, pp. 115–143.
Hilley, G.E., Arrowsmith, J.R., 2008. Geomorphic response to uplift along the Dragon's Back pressure ridge, Carrizo Plain, California. Geology 36, 367–370.
Hu, X., Wu, J., Wen, Z., Zhang, J., Zhao, Q., Pan, B., 2022. Fluvial evolution in a growing thrust-fold range of the Yumu Shan, NE Tibetan Plateau. Earth Planet. Sci. Lett. 594, 117704.
Hungr, O., Leroueil, S., Picarelli, L., 2014. The Varnes classification of landslide types, an update. Landslides 11, 167–194.
Islamova, S.K., Kazimova, S.E., Ismailova, S.S., 2019. Assessment of geodynamic risk of Mingachevir water reservoir. ANAS Trans. Earth Sci. 2, 61–69.
Ismail-Zadeh, A., Adamia, S., Chabukiani, A., Chelidze, T., Cloetingh, S., Floyd, M., Gorshkov, A., Gvishiani, A., Ismail-Zadeh, T., Kaban, M.K., Kadirov, F., Karapetyan, J., Kangarli, T., Kiria, J., Koulakov, I., Mosar, J., Mumladze, T., Müller, B., Sadradze, N., Safarov, R., Schilling, F., Soloviev, A., 2020. Geodynamics, seismicity, and seismic hazards of the Caucasus. Earth Sci. Rev. 207, 103222.
Jackson, J., Norris, R., Youngson, J., 1996. The structural evolution of active fault and fold systems in Central Otago, New Zealand: evidence revealed by drainage patterns. J. Struct. Geol. 18, 217–234.
Jarman, D., Harrison, S., 2019. Rock slope failure in the British Mountains. Geomorphology 340, 202–233.
Jibson, R.W., Prentice, C.S., Borissoff, B.A., Rogozhin, E.A., Langer, C.J., 1994. Some observations of landslides triggered by the 29 April 1991 Racha earthquake, Republic of Georgia. Bull. Seismol. Soc. Am. 84, 963–973.
Keefer, D.K., 1984. Landslides caused by earthquakes. Geol. Soc. Am. Bull. 95, 406–421.
Keller, E.A., Gurrola, L., Tierney, T.E., 1999. Geomorphic criteria to determine direction of lateral propagation of reverse faulting and folding. Geology 27, 515–518.
Kirby, E., Whipple, K.X., 2012. Expression of active tectonics in erosional landscapes. J. Struct. Geol. 44, 54–75.
Kirby, E., Harkins, N., Wang, E., Shi, X., Fan, C., Burbank, D., 2007. Slip rate gradients along the eastern Kunlun fault. Tectonics 26, TC2010.
Korup, O., 2004. Geomorphic implications of fault zone weakening: slope instability along the Alpine fault, South Westland to Fiordland. N. Z. J. Geol. Geophys. 47, 257–267.
Kotyuzhan, A.I., Molokov, L.A., 1990. A landslide near the abutment of the Mingechaur HES dam. Gidrotekhnicheskoe Stroitel'stvo 2, 28–30.
Larsen, I., Montgomery, D., 2012. Landslide erosion coupled to tectonics and river incision. Nat. Geosci. 5, 468–473.
Malamud, B.D., Turcotte, D.L., Guzzetti, F., Reichenbach, P., 2004. Landslide inventories and their statistical properties. Earth Surf. Process. Landf. 29, 687–711.
Matossian, A.O., Baghdasaryan, H., Avagyan, A., Igityan, H., Gevorgyan, M., Havenith, H.B., 2020. A new landslide inventory for the armenian lesser caucasus: slope failure morphologies and seismotectonic influences on large landslides. Geosciences 10, 111.
Miller, S.R., Baldwin, S.L., Fitzgerald, P.G., 2012. Transient fluvial incision and active surface uplift in the Woodlark Rift of eastern Papua New Guinea. Lithosphere 4, 131–149.
Montgomery, D.R., Brandon, M.T., 2002. Topographic controls on erosion rates in tectonically active mountain ranges. Earth Planet. Sci. Lett. 201, 481–489.
Moreiras, S.M., Sepúlveda, S.A., 2022. Landslides in arid and semi-arid environments. In: Shroder, J.J.F. (Ed.), Treatise on Geomorphology, vol. 5. Elsevier, Academic Press, pp. 322–337.
Mosar, J., Kangarli, T., Bochud, M., Glasmacher, U.A., Rast, A., Brunet, M.F., Sosson, M., 2010. Cenozoic-recent tectonics and uplift in the Greater Caucasus: a perspective from Azerbaijan. Geol. Soc. Lond. Spec. Publ. 340, 261–280.
Nalivkin, D.V., 1976. Geologic map of the Caucasus (in Russian): Ministry of Geology, Union of Soviet Socialist Republics, scale 1:500,000.
Nikonov, A.A., Nikonova, K.I., 1986. The strongest earthquake in Transcaucasia on September 30, 1139. In: Reconstruction by Historical, Historical-architectural and Archaeological Materials— Topics of Engineering Seismology, 27, pp. 152–183 (in Russian).
Pánek, T., Březný, M., Kapustová, V., Lenart, J., Chalupa, V., 2019. Large landslides and deep-seated gravitational slope deformations in the Czech Flysch Carpathians: New LiDAR-based inventory. Geomorphology 346, 106852.
Phillips, F.M., Meghraoui, M., 1983. Structural analysis and interpretation of the surface deformations of the El Asnam earthquake of October 10, 1980. Tectonics 2, 17–49.
Pierce, I., Guliyev, I., Yetirmishli, G., Muradov, R., Kazimova, S., Javanshiri, R., Johnson, B., Marshall, N., Walker, R., Wordsworth, P., in review. Surface rupturing earthquakes of the greater caucasus frontal thrusts, Azerbaijan, J. Geopys. Res. Solid Earth.
R Core Team, 2019. R: A Language and Environment for Statistical Computing.. RFoundation for Statistical Computing, Vienna, Austria.
Schwanghart, W., Scherler, D., 2014. Short communication: TopoToolbox 2 – MATLAB-based software for topographic analysis and modeling in Earth surface sciences. Earth Surf. Dyn. 2, 1–7.
Schwanghart, W., Scherler, D., 2017. Bumps in river profiles: uncertainty assessment and smoothing using quantile regression techniques. Earth Surf. Dyn. 5, 821–839.
Shirinov, F.A., Bajenov, Y.P., 1962. Geological Structure of the Southern Foothills of the Greater Caucasus [in Russian], Baku.
Sukhishvili, L., Forte, A.M., Merebashvili, G.L.J., Whipple, K.X., Javakhishvili, Z., Heimsath, A., Godoladze, T., 2021. Active deformation and Plio-Pleistocene fluvial reorganization of the western Kura fold–thrust belt, Georgia: implications for the evolution of the Greater Caucasus Mountains. Geol. Mag. 158, 583–597.
Tanyaş, H., Lombardo, L., 2019. Variation in landslide-affected area under the control of ground motion and topography. Eng. Geol. 260, 105229.
Tanyaş, H., vanWesten, C.J., Allstadt, K.E., Jibson, R.W., 2019. Factors controlling landslide frequency–area distributions. Earth Surf. Process. Landf. 44, 900–917.
Tebbens, S.F., 2020. Landslide scaling: a aeview. Earth Space Sci. 7, e2019EA00066.
Telesca, L., Kadirov, F., Yetirmishli, G., Safarov, R., Kazimova, S., 2018. Joint use of seismological and topological statistical methods for the analysis of 2010–2016 azerbaijan seismicity. Pure Appl. Geophys. 175, 4225–4239.
Tibaldi, A., Bonali, F.C, Pasquaré Mariotto, F., Tsereteli, N., Havenith, H.B., Babayev, G., Pánek, T. in review. Structural expression of the frontal thrust of an active fold-and thrust belt: The Holocene 123-km-long Kura Fault, Greater Caucasus, Azerbaijan. J. Struct. Geol.
Tibaldi, A., Ferrari, L., Pasquarè, G., 1995. Landslides triggered by earthquakes and their relations with faults and mountain slope geometry: an example from Ecuador. Geomorphology 11, 215–226.
Van Den Eeckhaut, M., Poesen, J., Govers, G., Verstraeten, G., Demoulin, A., 2007. Characteristics of the size distribution of recent and historical landslides in a populated hilly region. Earth Planet. Sci. Lett. 256, 588–603.
Yetirmishli, G.J., Mammadli, T.Y., Rzayev, A.G., Muradov, R.B., Kazimova, S.E., Garaveliyev, E.S., Ismayilova, S.S., Kazimov, I.E., Baghirov, E.M., 2018. Manifestation features of landslide process around the Mingachevir reservoir (2014). Seismoprogn. Observ. Territ. Azerb. 15, 3–13.